ELSEVIER

Chemical Geology 115 (1994) 173–211

CHEMICAL GEOLOGY
INCLUDING
ISOTOPE GEOSCIENCE

Crust and mantle contributions to granite genesis — An example from the Variscan batholith of Corsica, France, studied by trace-element and Nd–Sr–O-isotope systematics

A. Cocherie[a], Ph. Rossi[a], A.M. Fouillac[a], Ph. Vidal[b]

[a]*B.R.G.M., Service Géologique National, B.P. 6009, F-45060 Orléans Cedex 2, France*
[b]*C.N.R.S., U.A. No. 10, 5, rue Kessler, F-63038 Clermont-Ferrand Cedex, France*

(Received March 3, 1993; revision accepted December 20, 1993)

Abstract

The Corsican batholith, formed during the Variscan orogeny, was studied with particular emphasis on the respective roles played by crustal- and mantle-derived material in granite genesis. Major- and trace-element data identify: the various types of magma and their genetic relationships; the magmatic processes that gave rise to the observed rocks; and the primitive liquids. O–Sr–Nd-isotope systematics constrain the origin of primitive liquids. Trace-element models provide data on the various source materials and their possible geodynamic setting. The evolution of two main calc-alkaline plutonic associations is compared: an older high-Mg–K association (U_1) with both ultrapotassic mafic and silicic rocks, the latter ranging from monzonite to leucosyenogranite, and a younger calc-alkaline composite association (U_2) involving a mafic cumulate sequence and granodiorite to leucomonzogranite. Both types of granite are accompanied by mafic units that were non-cogenetic with surrounding granitic melts. Trace-element calculations indicate that a primitive liquid of monzodioritic composition gave rise to the U_1 Mg–K granite by fractional crystallization, amphibole and titanite playing a major role, which, with increasing crystallization, gave decreasing REE contents without a strong negative Eu anomaly. The U_2 calc-alkaline suite was formed by fractional crystallization involving feldspar and LREE-rich minerals, i.e. monazite, from a liquid of monzogranitic composition. Field and petrographical data identify magma mingling in both U_1 and U_2, between mafic and silicic rocks, but geochemical data only indicate how magma-mixing processes led to U_2 granodiorite. Geochemical modelling shows that a single protolith of calculated graywacke composition yielded the two associations under different melting conditions: the high-Mg–K monzodiorite melt was formed after partial melting of a 30% non-modal batch of granulite-facies metamorphic protolith (low p_{H_2O}), but the calc-alkaline monzogranite was formed by the same process in an amphibolite-facies source of similar composition (higher p_{H_2O}). The primitive granite magmas of both associations show the same crustal characteristics, i.e.: $Sr_i = 0.706–0.707$; $\epsilon_{Nd}(t) = -4.3$ to -2.2 and $\delta^{18}O = +7$ to $+8‰$. This provides evidence that the composition of both U_1 and U_2 granite melts probably was controlled by physico-chemical fusion rather than protolith-composition parameters. The U_1 ultrapotassic mafic rock is thought to be of mantle origin, i.e. a deep source containing phlogopite (±garnet). Zone refining led to a significant increase of incompatible trace-element contents during ascent of the magma. Mantle–crust interaction lowered the La/Yb and $^{143}Nd/^{144}Nd$ ratios, but the $^{87}Sr/^{86}Sr$ ratio increased. Nevertheless, interaction with associated U_1 Mg–K granite was not important and the crustal component is thought to be different from the associated granitic magma. In U_2, the mafic cumulate sequence, clearly of mantle origin, has E-MORB

[CA]

0009-2541/94/$07.00
SSDI 0009-2541(93)E0262-R

characteristics and seems the result of 10% non-modal partial melting of a heterogeneous mantle of spinel or amphibole peridotite without garnet. Some interaction occurred with the associated granitic melt. The E-MORB character of the mafic rock indicates that a large part of the batholith, and at least the U_2 magmatic association, was generated under post-collisional extensional conditions.

1. Introduction

The Variscan orogenesis was characterized by the emplacement of huge volumes of felsic magma of various compositions, whose origin is still strongly debated. References to Mesozoic or Cenozoic and present-day mountain chains, such as the Coast Range batholith or the Himalaya, provide neither a satisfactory model of tectonic setting, nor suitable explanations for the production and emplacement of such huge volumes of granite. The calc-alkaline trend, used to characterize magmatic suites or associations, is based on specific proportions of gabbro-diorite, tonalite-granodiorite and granite in a batholith, e.g., in the active margin batholith of Peru these proportions are 15:50:35 (Pitcher, 1979). In the Variscan batholith of Corsica, however, they are 3:15:82 (Orsini, 1980). Such contrasting proportions suggest different sources and/or melting processes. Furthermore, significant outcrops of Mg–K-enriched granitoid and/or ultrapotassic-mafic rocks are found in the "Moldanubian" southwestern branch of the Variscan orogen, where they are visible in certain external crystalline massifs of the Alps (Banzet, 1987). Similar plutons to the one found in northwestern Corsica, have been described from other parts of Variscan Europe, e.g., the Ballon Massif (southern Vosges: Pagel and Leterrier, 1980; Pagel, 1982) and the Bohemian Massif (Bouska et al., 1984), but their relationships (time of emplacement, composition of sources) with "normal" calc-alkaline trends remain to be clarified.

The aim of the present paper is to provide better constraints for a genetic model of the Variscan batholith found in Corsica, France, and Sardinia, Italy, and described by Rossi and Cocherie (1991). Considering the chemical evolution of the magmas produced in this batholith as well as their isotopic composition, it is possible to characterize: (1) the various types of magmatic association; (2) the magmatic processes; (3) the nature of initial liquids; (4) the sources; and (5) the existence of any inherited isotopic zonation or heterogeneities. This should clarify the respective roles played by reworking of continental crust and by input of mantle-derived material. The Variscan batholith of Corsica was a suitable target because of the existence of excellent outcrops of granite and associated mafic rock. Sampling was based on detailed field and petrographic studies by Marre et al. (1981).

2. Geological setting

The genesis of Mediterranean calc-alkalic plutonic associations was first studied in the Pyrénées and in the Corsican–Sardinian batholith through field work, petrography and major-element geochemistry. Most of this work was centred around two main hypotheses. The first (Autran et al., 1970; Marre, 1973) assumes that mafic and silicic rocks both resulted from the differentiation of a mafic magma. The second hypothesis (Leterrier, 1972; Debon, 1975; Orsini, 1980) favours mixing between mantle-derived and crustal components, and was based on trace-element (Fourcade and Allègre, 1981; Poli et al., 1989; Zorpi et al., 1991) and isotope-geochemistry (Allègre and Ben Othman, 1980; Michard-Vitrac et al., 1980; Ben Othman et al., 1984; Bickle et al., 1988) studies; these provided evidence for crustal anatexis in the formation of granitoid rock and for mixing between mantle-derived magma and crustal material in the genesis of mafic bodies.

The Variscan batholith of Corsica consists of plutons with distinct mineralogical and petrographic characteristics. Each unit was studied by the inverse geochemical approach (see Appendix B) through trace elements (Cocherie, 1986), before using isotope geochemistry. This ap-

proach favours the observation of data to identify the genetic processes that link the various samples belonging to a single unit, determining any genetic links between samples and examining the possible relationships between different units. Isotope data then constrain the model, especially in the search for source materials. A mineralogical and trace-element study (Cocherie et al., 1984; Rossi and Cocherie, 1991) of mafic and silicic intrusions into the Corsican calc-alkaline batholith, indicated that granite units represent batches of crustal anatexis. This work clearly showed that cumulate rocks of the mafic suite were produced by fractional crystallization of a mafic magma of mantle origin. In addition, hybridization phenomena were observed between the two end-members (Cocherie, 1984; Zorpi et al., 1991). This led Rossi and Chevremont (1987) to qualify such a plutonic association as a "calc-alkaline *composite*", suggesting a distinction from calc-alkaline rocks related to active margins.

The Corsica–Sardinia batholith (Fig. 1) resulted from the successive intrusion of three magmatic associations, U_1, U_2 and U_3, between Middle Carboniferous and Middle Permian times. Summarized mineralogical data on the rocks used for geochemical discussion are given in Appendix A; detailed petrographic and mineralogical data are available in Rossi (1986), and Rossi and Cocherie (1991).

The early U_1 Mg–K plutonic association is composed of biotite–amphibole–clinopyroxene–K-feldspar–megacryst-bearing monzonite to biotite–syenogranite, associated with ultrapotassic (Foley et al., 1987) mafic rock that forms < 10% of the association. Contacts between mafic and silicic Mg–K rocks are invariably plastic and show the same internal structure. The mafic bodies generally do not exceed 500 m in length and are commonly grouped in swarms. Rare lamprophyre dykes crosscutting the metamorphic basement near U_1 intrusions may be related to such ultra-K rocks. The U_1 association, emplaced with a N–S foliation trend during horizontal E–W shortening of the basement (Laporte, 1987), was dated (Cocherie et al., 1992) at 322 ± 12 Ma by $^{207}Pb^*/^{206}Pb^*$ on zircon with the stepwise-evaporation method (ZEM).

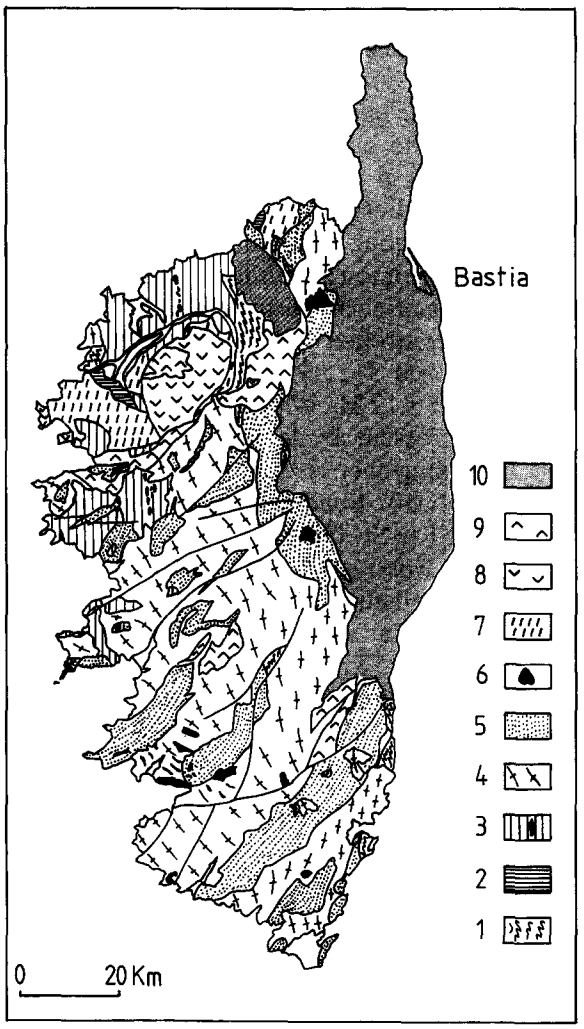

Fig. 1. Geological sketch map of the Corsican batholith. [*1*=metamorphic basement; *2*=Palaeozoic formations; *3*=U_1 Mg–K granitoid (*vertical stripes*) and ultra-potassic (*black patches*) rock; *4*=U_2 granodiorite and monzogranite (*oriented crosses* indicate trends of flow structures); *5*=U_2 leucomonzogranite; *6*=U_2 mafic and ultramafic rock; *7*=U_2 volcanic rock (andesite, dacite and rhyolite); *8*=U_3 alkalic volcanic rock; *9*=U_3 alkalic plutonic rock; *10*=post-batholithic formations].

The U_1 plutons were intruded by the U_2 volcanic–plutonic calc-alkaline "composite association". The U_1 and U_2 associations were then both cut by U_3 alkaline volcanic–plutonic intrusions, but these last intrusions will not be discussed here.

The U_2 volcanic–plutonic association is composed of both mafic and silicic bodies. Plutonic rocks outcrop widely and rare volcanic-rock roof pendants in the batholith, occur in NW Corsica. Intermediate to acidic plutonic-rock composition ranges from mafic microgranular enclave-bearing granodiorite, showing evidence of felsic–mafic mingling phenomena, to monzogranite and leucomonzogranite associated with mafic/ultramafic complexes (MUC). U_2 intrusions were controlled by NW–SE structures and gave ages from 312±9 Ma (Rb–Sr: Cocherie, 1984) to 305±12 Ma (ZEM: Rossi et al., 1993). They are crosscut by leucomonzogranite plutons, extending over several kilometres and controlled by N 050°-trending structures with an age of 290±6 (Rb–Sr; Cocherie, 1984) to 284±20 Ma (ZEM: Rossi et al., 1993). Mafic rocks of the U_2 calc-alkaline association occur as enclaves, septa or mafic/ultramafic complexes (MUC) up to 15 km^2 in size, and consist of cumulates of peridotitic, troctolitic and gabbronoritic composition; non-cumulates range in composition from gabbro-norite and olivine norite to diorite. The younger intrusions were dated around 278 Ma (ZEM: Rossi et al., 1992; Nd–Sm: Poitrasson et al., 1992).

Field, petrological and geochronological evidence indicates a link between plutonic and volcanic rocks, the MUC being regarded as magma chambers related to andesite (Rossi et al., 1992). Dacite, dated as 294±11 to 288±13 Ma (ZEM: Rossi et al., 1993) and with identical geochemical patterns as granodiorite of which it must be considered as the volcanic equivalent, was crosscut by leucomonzogranite.

3. Analytical methods

Major elements were determined by inductively coupled plasma atomic emission spectrometry (ICP–AES) at the C.R.P.G. (Nancy), using the Govindaraju et al. (1976) method. Trace elements, including Tb, were analysed by instrumental neutron activation (INAA) according to the method described by Chayla et al. (1973) and Jaffrezic et al. (1980), using an epithermal neutron flux with a Cd filter and an irradiation flux of $2.5 \cdot 10^{14}$ n cm^{-2} s^{-1}. For the rare-earth elements (REE), apart from Tb, we used a thermal and epithermal neutron flux of 10^{14} n cm^{-2} s^{-1}. The REE of most samples were determined with a radiochemical procedure, involving the separation of REE as a group after dissolving the irradiated powdered rocks (Treuil et al., 1973). All INAA work was done at the P. Süe laboratory (CEN Saclay).

Rb and Sr isotope data were determined at the CAESS at Rennes. Ages and initial Sr ratio calculations assumed an absolute error on measured $^{87}Sr/^{86}Sr$ of ±0.0002 (much higher than individual analytical errors) and a relative error on the $^{87}Rb/^{86}Sr$ ratio of ±2% (analytical technique: Jahn et al., 1980). Sm and Nd isotope data were determined at the University of Clermont-Ferrand (technique: Deniel et al. (1987). La Jolla standard runs gave a $^{143}Nd/^{144}Nd$ ratio of 0.511858±0.000009 (2σ). $^{18}O/^{16}O$ ratios were measured at B.R.G.M. (Orléans) after gas extraction by routine BrF_5 techniques (Clayton and Mayeda, 1963). The average reproducibility of isotope analyses is better than ±0.2‰.

Single-zircon dating by ZEM was done on a Finnigan® Mat *261* mass spectrometer at B.R.G.M. (Orléans), using an analytical technique described by Cocherie et al. (1992)

4. Definition of U_1 and U_2 units, using major and trace elements

All major- and trace-element analyses of U_1 and U_2 rocks are available either in Tables 1 and 2, or in Cocherie et al. (1984). The A/CNK ratio of 1.1–1.3 in whole-rock acidic samples of both U_1 and U_2 associations characterizes their slight peraluminous bulk composition (Shand, 1927). Oxide trends are plotted in Fig. 2; they enable a fairly clear distinction between U_1 and U_2 samples, except for rock with an SiO_2 content of >65%, whose composition is close to minimum melts in the granite system. It is interesting to note that U_2 leucocratic granite has a much lower Sr and Co content than similar high-SiO_2 U_1 rock (Fig. 3). Moreover, the Fe content of

biotite, which is lower in U_1 ($X_{Fe} \approx 0.5$) than in U_2 ($X_{Fe} \approx 0.8$–0.9), is another effective discriminating criterion (Rossi and Chevremont, 1987). Contrasting trends in the low-silica-content range of both U_1 and U_2 units emphasize the role played by mineral fractionation as indicated by textural evidence (Rossi, 1986).

4.1. *Mg–K association of* U_1 *rocks*

Major elements display smooth variations that fit rather straight lines in projections (Harker, 1909), suggesting a linkage between mafic and silicic end-members. The fairly constant alkali sum is controlled by both ferromagnesian minerals and K-feldspar, whose abundance respectively decreases and increases from the mafic to acidic apexes. Covariance of this ratio with Cr+Ni strongly suggests that enrichment in K_2O was primary (Thompson et al., 1990). TiO_2 and P_2O_5 trends are related to fractionation of accessory minerals such as apatite and/or titanite. The K_2O/Na_2O ratio in mafic rock characterizes high- to ultra-potassic compositions (Foley et al., 1987). U_1 is richer in alkali, MgO and TiO_2, and poorer in CaO and Fe_2O_3 than the U_2 association, and can be compared to classical high-K calc-alkaline plutonic "suites".

Trace-element distribution of the two suites indicates that U_1 Mg–K plutonism was characterized by enrichment in transition metals (Sc, Cr, Co, Ni) and by high concentrations of large-ion lithophile elements (LILE: Rb, Cs, Sr, Ba) as well as high contents of elements with small highly charged ions (U, Th, Ta, Hf, Zr). With increasing SiO_2, the U_1 association shows a strong decrease of Sc, Cr, Co, Ni, Sr, Ba, Hf and Zr contents, whereas Rb and Th slightly increase towards the leucocratic facies. For example, the Co vs. Th and Sr vs. Rb variations in Fig. 3 clearly indicate the particular location of the Corsican Mg–K field, which mostly includes the representative points of Mg–K "durbachitic" Bohemian plutonism (Cocherie and Rossi, 1991) and is far from the U_1 calc-alkaline field. All samples (Fig. 4), including mafic rock, exhibit strong REE fractionation (La/Yb=36). Most patterns have a weakly negative Eu anomaly ($Eu/Eu^{\star}=0.75$). The total REE content is generally high and decreases from mafic to acidic rocks (ΣREE 100–665 ppm), with a high average value in mafic rock (ΣREE=450 ppm) and a quite "common" average value in Mg–K granitoid rock (ΣREE=200 ppm). The more siliceous the samples, the more concave are their heavy REE (HREE) distribution patterns. Trace-element data for mafic rocks of the U_1 Mg–K association show great similarity with data from calc-alkaline lamprophyre with high REE, Rb, Sr and Ba concentrations.

4.2. U_2 *acidic and intermediate rocks*

U_2 granodiorite shows two types of REE pattern (Fig. 5a) with a constant ΣREE of 150 ppm: (1) More acidic granodiorite (Cocherie et al., 1984) has strongly fractionated patterns (La/Yb $\approx$ 25), but less than for Mg–K granitoid rock, and no Eu anomaly is seen. (2) More intermediate granodiorite has less fractionated light REE (LREE) patterns, more HREE-enriched patterns and a negative Eu anomaly. Less acidic granodiorite has the most pronounced Eu anomalies, which is unusual compared with the general differentiation trend of granitic magma according to a fractional crystallization model; this point will be discussed in Section 7.4. U_2 monzogranite shows a regular variation in REE distribution as a function of SiO_2 content (Fig. 5b). The LREE patterns are fractionated, but no Eu anomaly appears for the less siliceous monzogranite (see CLB *13*); this pattern is similar to that of highly siliceous granodiorite (see PR *7* and CLB *10*). Rather flat REE patterns with low LREE and a strongly negative Eu anomaly characterize leucocratic bodies (e.g., CLB *63*). At present, most authors (Cocherie, 1978; Fourcade and Allègre, 1981; Vidal et al., 1982; Gromet and Silver, 1983; Mittlefehldt and Miller, 1983; Vidal et al., 1984) recognize that accessory phases (e.g., allanites, monazites) probably trap the LREE during late stages of differentiation.

Table 1
Major- (in % oxides) and trace-element (in ppm) concentrations in U_1 high-Mg–K rocks of Corsica

	Syenomonzonites							Monzodiorites – monzogranites		
	K *1*	K *5*	K *4*	K *6*	K *25*	K *2*	K *18*	*1*	*2*	*3*
SiO_2	42.30	48.30	49.20	51.00	52.60	53.60	57.30	60.48	64.46	64.03
Al_2O_3	12.10	17.30	13.00	14.10	12.30	15.20	16.10	16.50	16.08	15.99
Fe_2O_3[a]	13.04	8.77	6.90	8.56	7.22	7.91	6.68	5.29	4.23	4.18
MnO	0.18	0.12	0.10	0.13	0.11	0.10	0.10	0.07	0.06	0.06
MgO	12.90	6.65	8.80	7.30	10.50	6.05	4.70	2.58	1.78	1.81
CaO	6.90	6.55	5.50	7.00	6.80	5.75	5.30	3.74	3.21	3.26
Na_2O	0.70	2.45	2.10	2.50	1.85	2.80	2.70	3.40	3.44	3.87
K_2O	5.40	4.40	7.90	4.90	4.70	3.60	4.00	4.94	4.49	4.40
TiO_2	2.65	2.25	2.15	1.60	1.15	1.90	1.40	1.11	0.79	0.79
P_2O_5	1.00	1.00	1.90	1.50	1.15	1.00	0.50	0.38	0.25	0.24
LOI	2.25	1.40	0.70	0.95	1.35	1.15	1.10	1.27	1.39	1.42
Total	99.42	99.19	98.25	99.54	99.73	99.06	99.88	99.44	99.94	99.81
U	4.4	3.9	4.9	4.7	6.3	4.4	4.9	4.3	7.9	6.3
Th	27.0	20.5	29.0	17.8	24.3	12.6	19.4	19.7	21.4	21.7
Ta	0.76	3.46	3.44	1.31	0.78	1.09	1.32	2.04	2.39	2.18
Hf	12.5	15.1	28.8	11.2	11.7	7.51	8.82	9.70	7.81	8.81
Zr	465	600	1,199	524	504	331	341	405	352	373
Sc	31.3	25.4	20.8	25.7	21.0	17.6	18.5	11.4	9.07	9.18
Cr	673	163	325	233	562	239	77	69	39	39
Co	54	30	29	30	36	28	21	11.7	9.7	4.5
Ni	341	57	138	175	286	83	22	26	17	17
Zn	148	113	105	133	89	95	74	72	55	63
Cs	15.7	3.44	5.42	5.23	9.19	4.06	7.57	4.64	4.76	4.59
Rb	412	203	288	248	197	159	165	201	193	170
Sr	67	1,182	1,242	1,173	1,401	1,067	515	683	533	569
Ba	1,556	2,419	6,410	2,991	3,324	2,082	1,602	1,675	1,334	1,360
La	53.9	97.9	156	126	86.7	62.0	51.3	62.2	58.3	63.4
Ce	101	216	296	261	178	121	100	135	130	130
Nd	–	116	150	–	111	–	52.1	61.3	54.9	67.0
Sm	11.5	18.7	22.1	32.4	20.0	11.9	9.2	10.8	9.14	11.5
Eu	2.14	4.23	5.10	5.14	4.56	2.64	1.87	2.00	1.76	2.07
Gd	–	–	–	–	–	–	–	7.89	6.88	–
Tb	0.72	1.51	1.46	2.21	1.47	0.82	0.89	0.94	0.77	0.98
Dy	–	–	–	–	–	–	–	5.14	4.36	–
Er	–	–	–	–	–	–	–	2.33	2.18	–
Yb	1.61	3.67	2.60	4.08	2.49	1.53	2.73	1.99	2.04	2.48
Lu	–	–	–	–	–	–	–	0.27	0.26	–
ΣREE[b]	249	491	665	643	431	287	241	306	286	302
La/Yb	34	27	60	31	35	41	19	31	29	26
Eu/Eu*	0.79	0.88	0.96	0.65	0.92	0.91	0.75	0.71	0.82	0.69
Th/U	6.1	5.3	5.9	3.8	3.9	2.9	4.0	4.6	2.7	3.4
Th/Ta	36	5.9	8.4	14	31	12	15	10	9.0	10
Zr/Hf	37	40	42	47	43	44	39	42	45	42

LOI = loss on ignition; Eu* = interpolated value of Eu.
[a] Fe_2O_3 = total Fe as Fe_2O_3.
[b] ΣREE = total REE content with interpolated values.

K 20	K 22	K 24	5	8	K 12	4	6	K 13	7	K 21
66.30	71.50	71.50	71.43	72.46	74.30	73.14	74.80	75.20	74.69	75.05
15.80	14.10	14.30	13.75	13.63	12.80	13.26	12.55	13.50	13.12	13.45
3.34	2.18	2.18	2.17	2.24	1.71	1.82	1.51	1.18	1.20	1.33
0.05	0.04	0.03	0.04	0.05	0.03	0.03	0.04	0.03	0.03	0.03
1.80	1.15	1.10	0.41	0.81	0.60	0.65	0.96	0.50	0.33	0.40
2.50	1.15	1.55	1.67	1.74	1.30	1.58	1.09	0.90	1.19	1.28
2.75	3.15	3.40	2.92	3.36	3.00	3.44	4.06	3.25	3.61	3.89
5.30	4.60	4.20	4.69	4.67	4.70	4.20	4.32	4.35	4.60	3.66
0.55	0.30	0.35	0.38	0.39	0.25	0.32	0.24	0.12	0.18	0.16
0.25	0.10	0.17	0.12	0.11	0.10	0.09	0.07	0.05	0.05	0.06
0.50	0.70	0.35	1.00	0.58	0.40	0.74	0.66	0.42	0.61	0.52
99.14	98.97	99.13	98.46	99.91	99.19	99.16	100.21	99.50	99.53	99.83
3.6	12.3	2.7	5.6	5.7	11.9	6.9	11.7	15.0	9.9	8.9
26.8	26.8	19.3	38.1	49.0	45.9	49.4	41.8	33.2	32.9	22.0
0.91	1.82	1.29	2.01	2.09	1.76	1.55	1.88	1.74	1.74	0.91
8.73	4.13	3.94	5.03	5.30	4.04	4.34	4.97	3.75	2.87	2.98
309	149	146	190	216	143	184	153	115	91	104
7.49	4.99	4.54	4.32	4.26	3.37	3.23	3.36	4.18	2.44	3.40
47	31	25	16	16	13	10	7	7	5	11
7.5	4.5	3.8	1.0	3.5	2.4	12.7	2.2	1.3	1.5	2.1
13	9.5	7.4	7.9	7.8	6.1	5.4	4.1	3.2	3.3	4.2
59	51	44	39	44	28	32	26	19	25	32
11.4	8.15	13.5	5.60	5.16	4.68	3.50	4.39	9.94	3.77	9.76
203	231	196	221	204	239	179	222	316	235	204
513	304	343	356	344	192	308	192	111	204	283
1,248	784	833	825	750	370	526	387	240	320	260
72.8	38.8	30.7	56.4	52.0	44.5	46.7	39.5	23.5	32.4	27.4
133	73.9	59.9	95.0	105	77.3	72.5	65.0	42.7	57.6	46.7
–	28.8	23.1	–	37.0	20.6	–	–	–	16.6	–
8.3	4.9	4.2	6.0	5.70	2.9	3.5	2.2	3.4	2.39	2.6
1.64	0.95	1.10	1.09	0.99	0.61	0.79	0.57	0.43	0.50	0.55
–	–	–	–	3.73	–	–	–	–	1.79	–
0.58	0.51	0.48	0.49	0.45	0.29	0.31	0.24	0.12	0.18	0.22
–	–	–	–	2.80	–	–	–	–	1.26	–
–	–	–	–	1.50	–	–	–	–	0.76	–
1.36	1.51	0.99	1.59	1.45	1.20	0.96	1.02	0.89	0.89	0.40
–	–	–	–	0.21	–	–	–	–	0.16	0.07
293	167	136	217	222	163	162	138	98	120	103
54	26	31	36	36	37	49	39	26	36	69
0.81	0.69	0.91	0.71	0.72	0.76	0.85	0.91	0.65	0.69	0.83
7.4	2.2	7.2	6.8	8.6	3.9	7.2	3.6	2.2	3.3	2.5
30	15	15	19	23	26	32	22	19	19	24
35	36	37	38	41	35	42	31	31	32	35

Table 2
Major- (in % oxides) and trace-element (in ppm) concentrations in U_2 association and metamorphosed rocks of Corsica

	Peridotite	Troctolites		Gabbros				Monzogranites			
	PC *6*	PC *7*	PC *4*	PC *5*	P *6*	P *1*	*532*	CLB *72*	CLB *77*	CLB *76*	CLB *78*
SiO_2	40.40	45.30	47.00	48.00	45.00	48.20	47.20	74.63	74.74	74.80	75.43
Al_2O_3	10.40	22.30	26.10	15.30	14.40	16.70	18.10	13.34	13.27	12.82	13.44
Fe_2O_3[a]	11.64	7.09	4.19	11.67	15.17	11.32	11.32	2.28	2.25	2.81	2.03
MnO	0.17	0.10	0.06	0.20	0.25	0.20	0.15	0.04	0.05	0.07	0.05
MgO	26.60	10.60	6.35	7.00	7.40	7.10	8.11	0.19	0.25	0.31	0.22
CaO	4.75	11.00	12.55	10.20	12.0	9.50	11.90	1.35	1.43	1.47	1.40
Na_2O	0.75	1.70	2.15	3.10	2.90	2.75	1.38	2.86	2.77	3.00	2.55
K_2O	0.07	0.10	0.07	0.55	0.25	0.65	0.29	4.90	4.95	4.06	5.02
TiO_2	0.48	0.20	0.25	2.00	1.95	1.70	0.81	0.18	0.16	0.24	0.16
P_2O_5	0.06	0.03	0.04	0.25	0.35	0.45	0.06	–	–	–	–
LOI	4.95	1.35	0.75	1.20	0.30	0.85	0.65	0.32	0.28	0.36	0.27
Total	100.27	99.77	99.51	99.47	99.97	99.42	99.97	100.09	100.15	99.94	100.57
U	0.05	0.03	0.01	0.28	0.02	0.38	0.16	2.4	4.2	7.2	3.3
Th	0.17	0.16	0.11	0.97	0.34	1.31	0.77	13.4	15.3	22.1	13.9
Ta	0.11	0.05	0.04	0.52	0.18	0.82	0.12	0.86	1.18	1.96	1.12
Hf	0.73	0.30	0.46	4.28	2.56	4.07	0.90	4.48	3.48	4.94	3.50
Zr	25	13	26	208	136	179	41	163	126	169	116
Sc	11.0	7.7	5.3	37	49	30	32.5	3.6	3.7	4.7	3.6
Cr	2,040	480	191	262	252	154	149	–	–	–	–
Co	102	46	28	42	50	39	47	2.9	3.6	3.5	3.7
Ni	1,008	265	144	64	16	121	53	–	–	–	–
Zn	71	44	26	93	112	115	81	61	40	104	39
Cs	0.27	0.03	0.05	0.79	0.14	0.45	0.18	2.8	3.8	4.2	3.5
Rb	1.6	0.5	0.5	19.5	1.5	12	7.3	144	181	179	183
Sr	–	388	429	264	490	283	330	77	91	79	90
Ba	15	30	37	95	202	122	81	402	501	335	440
La	1.8	1.9	1.5	11.3	10.4	25.7	5.2	37.2	34.8	40.0	33.1
Ce	4.6	4.7	3.8	27.9	24.8	57.7	10.4	68.7	63.8	74.5	59.3
Nd	3.3	3.1	4.0	19.0	18.0	35.0	–	–	–	–	–
Sm	1.33	0.59	0.71	5.32	5.45	8.05	1.53	5.10	4.92	6.14	4.75
Eu	0.48	0.49	0.46	1.90	2.73	1.75	0.58	0.76	0.78	0.74	0.75
Gd	1.18	0.55	0.48	6.06	5.67	6.42	–	–	–	–	–
Tb	0.21	0.09	0.11	1.02	0.93	1.26	0.25	0.52	0.61	0.83	0.64
Tm	0.19	–	–	–	–	0.53	–	–	–	–	–
Yb	0.91	0.33	0.43	3.20	2.32	4.42	0.90	1.92	2.61	3.90	2.79
Lu	0.18	0.06	0.07	0.45	0.31	0.75	–	–	–	–	–
ΣREE[b]	18	14	12	92	87	158	31	160	154	184	146
La/Yb	20	5.8	3.5	3.5	4.5	5.8	5.8	19.4	13.3	10.3	11.9
Eu/Eu*	1.26	2.70	2.60	1.05	1.52	0.76	1.17	0.55	0.55	0.40	0.55
Th/U	3.4	5.3	11	3.5	17	3.5	4.8	5.6	3.6	3.1	4.2
Th/Ta	1.6	3.2	2.8	1.0	1.9	1.6	6.4	15.6	13.0	11.3	12.4
Zr/Hf	34	43	57	49	53	44	46	36	36	34	33

LOI = loss on ignition; Eu* = interpolated value of Eu.
[a] Fe_2O_3 = total Fe as Fe_2O_3
[b] ΣREE = total REE content with interpolated values.

Leucocratic monzogranites					Granulitic paragneiss				
CLB *69*	CLB *68*	CLB *75*	CLB *61*	CLB *62*	SL *35*	SL *18*	SL *22*	SL *20*	SL *21*
75.09	75.23	74.90	75.98	77.14	50.40	52.00	59.70	66.50	66.70
13.40	13.27	13.23	12.48	12.49	18.80	18.20	16.80	16.00	15.70
2.32	2.08	1.76	1.54	1.42	13.31	13.16	9.05	6.04	5.64
0.07	0.07	0.07	0.06	0.06	0.18	0.19	0.14	0.11	0.11
0.29	0.24	0.08	0.03	0.03	6.15	6.15	4.20	2.70	2.40
1.38	1.44	0.99	0.63	0.56	3.40	3.25	3.00	2.70	2.40
3.24	3.48	3.20	3.32	3.04	2.30	2.15	2.60	2.80	3.10
4.10	4.10	4.87	4.96	4.58	1.50	1.30	1.40	1.60	1.85
0.23	0.23	0.11	0.06	0.01	1.10	1.05	0.85	0.45	0.50
–	–	–	–	–	–	–	–	–	–
0.48	0.44	0.52	0.35	0.52	2.22	1.95	1.84	1.35	1.44
100.60	100.58	99.73	99.41	99.84	99.36	99.40	99.58	100.25	99.89
7.9	4.0	6.7	14.2	11.2	0.7	0.8	0.6	0.3	0.5
18.8	16.2	23.9	32.1	26.9	10.6	11.8	15 9	7.03	8.51
2.28	2.22	2.08	3.21	4.13	1.10	1.05	1.09	1.05	1.22
3.81	3.79	3.55	3.89	3.67	9.74	9.71	7.52	4.00	4.16
133	130	107	92	87	377	359	301	183	182
5.0	4.7	4.1	3.2	3.0	35.6	36.6	28.2	21.3	18.8
–	–	–	–	–	182	171	88	33	27
3.3	3.7	2.7	1.9	1.9	111	112	125	134	130
–	–	–	–	–	94	87	37	6.7	5.9
42	38	49	57	69	163	159	99	62	57
6.0	8.5	7.8	5.8	8.0	0.29	0.27	0.41	0.49	0.50
188	215	271	311	348	41	37	43	43	43
90	88	47	24	24	306	295	109	290	225
451	410	215	98	115	362	362	579	403	549
29.2	30.0	20.8	19.6	17.8	48.1	48.1	50.8	32.6	37.2
55.8	56.9	42.6	44.1	41.0	80.8	79.0	83.1	51.8	58.6
–	–	–	–	–	–	–	–	–	–
4.76	5.04	5.34	6.09	6.32	6.63	6.84	6.59	4.06	4.55
0.63	0.70	0.55	0.33	0.35	1.76	1.59	1.76	2.00	1.91
–	–	–	–	–	–	–	–	–	–
0.82	0.81	1.08	1.28	1.55	2.06	2.20	1.59	1.23	1.08
–	–	–	–	–	–	–	–	–	–
3.33	3.39	5.65	6.79	8.69	6.52	6.69	5.85	4.62	3.75
–	–	–	–	–	1.05	0.93	0.86	1.05	0.65
141	145	126	135	137	224	225	223	146	157
8.8	8.9	3.7	2.9	2.1	7.4	7.2	8.7	7.1	7.3
0.41	0.44	0.30	0.15	0.15	0.66	0.57	0.72	1.24	1.14
2.4	4.1	3.6	2.3	2.4	15.1	14.8	26.5	23.4	17.0
8.3	7.3	11.5	10.0	6.5	9.6	11.2	14.6	6.7	7.0
35	34	30	24	24	39	37	40	46	44

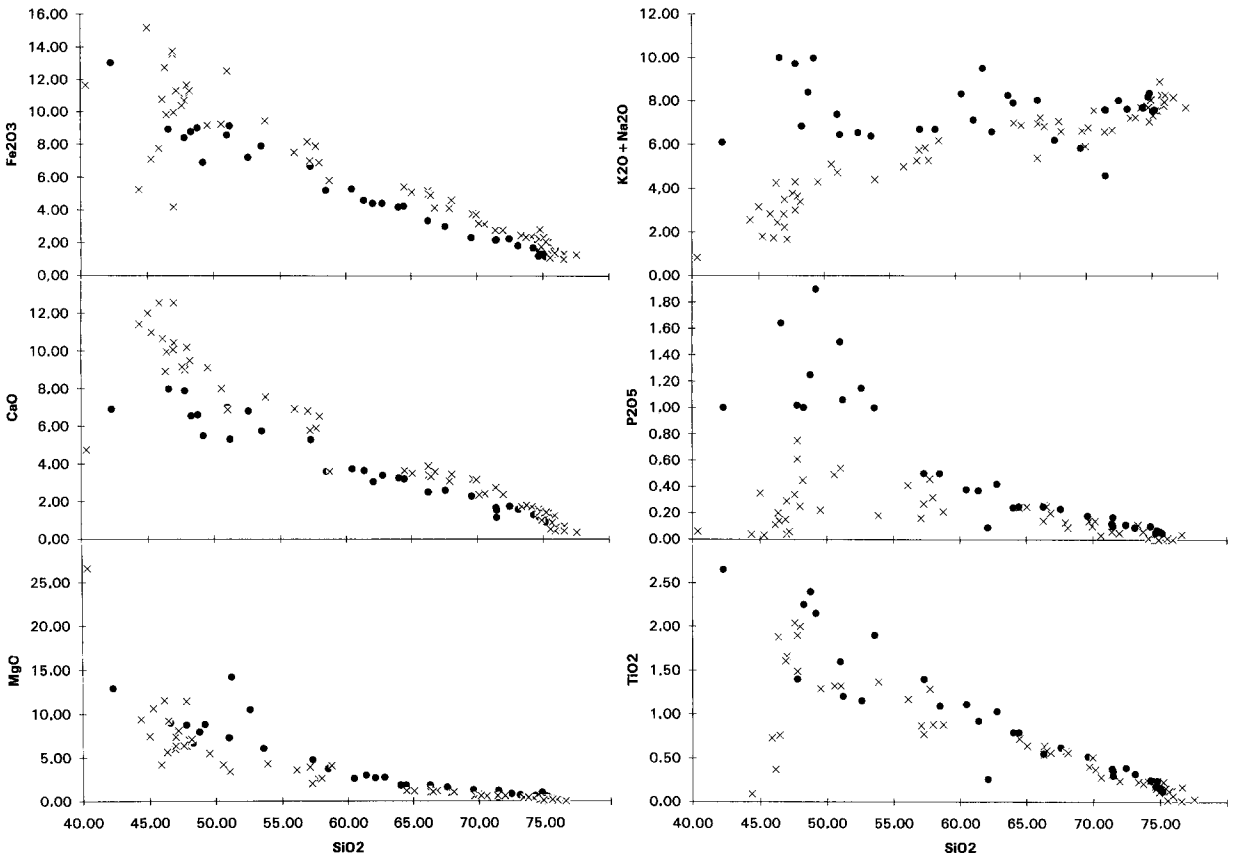

Fig. 2. Plot of some major oxides against SiO_2 (*solid circles* = U_1 Mg–K calc-alkaline plutonic association; *crosses* = U_2 composite calc-alkaline plutonic association). Sources of data: Orsini (1980) and this work; Cocherie et al. (1984); and Laporte (1987).

4.3. U_2 *mafic rocks*

Textural evidence of mainly olivine and/or plagioclase cumulative processes in mafic and ultramafic rocks (Cocherie et al., 1984; Rossi, 1986) is emphasized by the contrasted disposition of clouds of major oxides, with CaO indicating the dominant role of plagioclase fractionation (Fig. 2). Troctolite shows a slightly fractionated pattern with a well-developed positive Eu anomaly ($Eu/Eu^{\star}=3$) at very low concentration levels, corresponding to the modal composition of such rock that mainly consists of cumulate plagioclase (Fig. 6a). Gabbro-norite, also of cumulative origin, has low REE concentrations ($\Sigma REE=30$–40 ppm) with a very weak positive Eu anomaly. The least differentiated gabbro, corresponding to primary magma, has a higher REE content ($\Sigma REE=70$–90 ppm) than the cumulate, no or a weak negative Eu anomaly, and slightly LREE-enriched patterns (Fig. 6a and b). The other mafic rocks (gabbro and diorite) are considered as differentiates of this cogenetic suite (Cocherie, 1986); they generally show a negative Eu anomaly and REE enrichment. However, detailed trace-element investigations show exceptions to this general cogenetic evolutionary trend: some rocks of nearly equal initial liquid composition have higher HREE contents as well as slight enrichment of other incompatible elements (e.g., Ta). This may reflect a heterogeneity of the mantle source, a point that will be discussed in more detail in Section 7.2. Gabbro considered as a product of a primary melt,

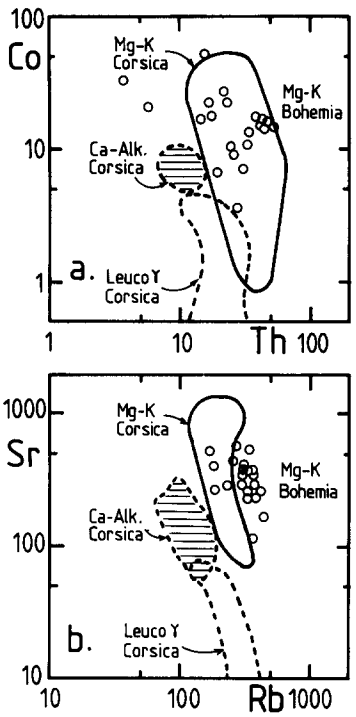

Fig. 3. a. Logarithmic plot of Co (ppm) against Th (ppm). b. Logarithmic plot of Sr (ppm) against Rb (ppm). U_1 Mg–K rock is compared with a similar association outcropping in Bohemia and with the U_2 calc-alkaline association from the Corsican batholith.

ranges in composition (major and trace elements, see REE patterns on Fig. 6b) from high-Al basalt (Philpotts et al., 1971; Cole et al., 1983; Crawford et al., 1987) to tholeiitic basalt (Jakes and Gill, 1970; Nicholls et al., 1980; Cullers and Graf, 1984).

Trace-element patterns clearly define the various groups of rock defined by field and petrographic studies. Their contrasting distributions do not contradict any hypothesis of formation from different sources for silicic and mafic end-member compositions. However, the gap in intermediate composition, observed around 55% SiO_2 in U_1, and between 60% and 65% SiO_2 in U_2 trends (Fig. 2), is not related to undersampling, but could indicate that the end members of each association have different origins. Isotope composition should be a useful tool for better definition of possible protolith origin.

5. Isotope data

The Sr, Nd and O isotope data are listed in Table 3.

5.1. Rb–Sr isotope data

Ten monzodiorite–monzogranite samples from the U_1 Mg–K association define a Rb–Sr whole-rock regression line (Fig. 7a), which corresponds to an age of 297 ± 8 Ma and an initial $^{87}Sr/^{86}Sr$ ratio of 0.7071 ± 0.0002. In spite of the low MSWD (1.6), the whole-rock regression age cannot be considered as the age of the U_1 unit, since single-zircon dating gives an average age of 322 ± 12 Ma (Cocherie et al., 1992), which agrees with field evidence (Marre and Rossi, 1981). The regression line of Fig. 7a is considered as a mixing line between monzogranite with a low $^{87}Rb/^{86}Sr$ (~ 1) and younger leucocratic monzogranite that was emplaced somewhat later and has a higher $^{87}Rb/^{86}Sr$ (> 3). Acid–mafic interaction would have given older Rb–Sr ages, since the less radiogenic mafic components have lower Rb/Sr and $^{87}Sr/^{86}Sr$ initial ratios, which means that this type of interaction can be considered as insignificant. Five of the six syenomonzonites plotted on Fig. 7a have lower age-corrected (322 Ma) $^{87}Sr/^{86}Sr$ ratios, ranging from 0.7046 to 0.7064, and thus fall below the isochron, whereas the sixth (0.7081) plots above it. This indicates that the mafic rock must be considered as non-cogenetic with the granite.

Twelve monzogranite samples from the U_2 calc-alkaline association define a regression line (Cocherie et al., 1992) yielding an age of 312 ± 9 Ma and an initial $^{87}Sr/^{86}Sr$ ratio of 0.7065 ± 0.0004. This age is interpreted as the time of emplacement of the calc-alkaline suite, and is supported by a single-zircon age determination (305 ± 12 Ma; Rossi et al., 1993). The leucocratic monzogranite that crosscuts U_2 monzogranite, provides another regression line (Cocherie et al., 1992) giving a younger age of 290 ± 6 Ma and an initial $^{87}Sr/^{86}Sr$ ratio of 0.7057 ± 0.0011. Single-zircon dating by step-

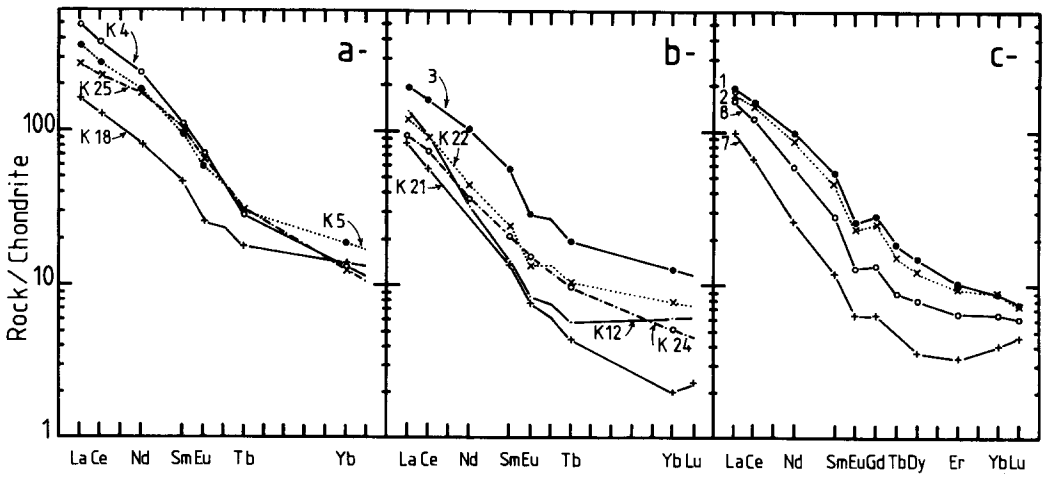

Fig. 4. Representative chondrite-normalized REE patterns of Mg–K rock: (a) basic rock (syenomonzonite); and (b) and c) monzodiorite to monzogranite.

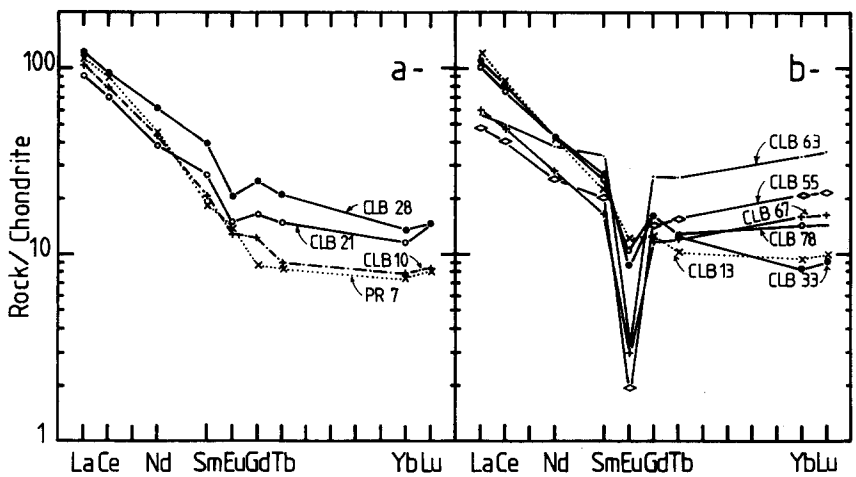

Fig. 5. Representative chondrite-normalized REE patterns of the U_2 calc-alkaline suite.
a. Granodiorite consists of two main groups of samples: one (CLB *10*, PR *7*) with no Eu anomaly, and the other (CLB *28*, CLB *21*) with a negative Eu anomaly.
b. Variation from monzogranite to leucocratic monzogranite leads to decreasing LREE and increasing HREE contents, with an increasingly negative Eu anomaly.

wise Pb evaporation on leucomonzogranite of northern Corsica (Rossi et al., 1993) gave an age of 284 ± 20 Ma, indicating that emplacement of this huge granite batholith may have taken at least 10 Ma. The representative points (13 samples) of U_2 granodiorite do not define an isochron, as most lie slightly above the monzogranite reference isochron (Fig. 7b) and some have lower $^{87}Sr/^{86}Sr$ ratios. Nevertheless, all acidic granitoid rocks display a rather constant $^{87}Sr/^{86}Sr$ initial ratio around 0.7065, which is significantly less radiogenic than other European Hercynian plutonic rocks, e.g., the Pyrénées (Michard-Vitrac et al., 1980; Bickle et al., 1988; Cocherie et al., 1994) or Sardinia (Brotzu et al., 1983; Cocherie, 1984; Bouchet et al., 1992)

Mafic rock from the U_2 calc-alkaline complex is plotted in Fig. 7c. Some plots scatter around the monzogranite reference isochron, whereas troctolite and some gabbros are far below it, thus

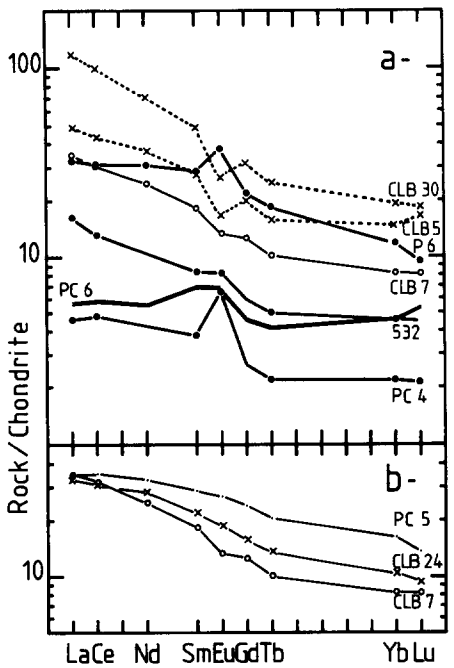

Fig. 6. Representative chondrite-normalized REE patterns of basic rock associated with the U_2 calc-alkaline suite.
a. *Solid line* and *full circles*=cumulates (PC *4*, *532*, P *6*); *open circles*=gabbro corresponding to a possible initial melt (CLB *7*); *dashed lines*=gabbro (CLB *5*) and diorite (CLB *30*) corresponding to differentiated melt; *double line*=peridotite (PC *6*).
b. Three possible initial melts of gabbroic composition.

indicating a different origin for these rocks from that of acidic granitoid rock.

5.2. Sm–Nd isotope data

Although two isochrons were obtained using the Rb–Sr method on U_2 granitoid rock, no $^{143}Nd/^{144}Nd$ vs. $^{147}Sm/^{144}Nd$ isochron can be drawn. This may be due to an absence of isotopic homogenization of Nd isotopes on the scale of the batholith, but is also partly due to the relatively young age of the granitoid complex and the narrow range of variation of Sm/Nd ratios, compared to the range of Rb/Sr ratios. Field relationships and a Sm–Nd isochron from one of the MUC (Fozzano–Peloso) led Poitrasson et al. (1992) to calculate young ages between 285 and 263 Ma, which agrees with the 280-Ma ZEM age determined by Rossi et al. (1992). The data are shown on a $(^{87}Sr/^{86}S)_i$ vs. $\epsilon_{Nd}(t)$ diagram (Fig. 8). Two groups are seen: most samples indicate a crustal origin, but some mafic rocks show mantle affinity. Moreover, it is not possible to distinguish between U_1 and U_2 granitic rocks on such a diagram.

5.3. Oxygen isotope data

U_1 and U_2 rocks give similar $\delta^{18}O$-values, ranging from +5.1 to +8.9‰ for U_2 and from +5.9 to +8.2‰ for U_1 Mg–K. For acidic rock, these values are slightly lower than those of common rock-types of the same composition in other Variscan intrusions (Sheppard, 1986).

U_2 rocks show a regular increase of $\delta^{18}O$ from +5.1 to +7.8‰ in mafic rock, +7.4 to +8.0‰ in granodiorite, +7.4 to +8.3‰ in monzogranite and +8.4 to +8.9‰ in leucomonzogranite. The lack of gap between mafic and acidic rocks suggests either a cogenetic relationship between mafic and silicic rocks, i.e. the latter deriving from the former, or that hybridization processes bridged the gap between each end-member. The isotope fractionation observed between mafic and acidic terms (3‰) is too large to be only the result of fractional crystallization; this is clearly shown on Fig. 9, where whole-rock $\delta^{18}O$-values are plotted against SiO_2 contents used as a differentiation index. The trend is compared to that observed for the oceanic Ascension island, South Atlantic, where a fractionation trend of < 1.5‰ is considered as a good estimate of O isotope behaviour accompanying fractional crystallization (Weiss et al., 1987). The difference between these two fractionation trends is too large to be attributed to temperature differences between plutonic and volcanic processes. These results imply that the U_2 association was created by two different magma batches. The high $\delta^{18}O$-values of some mafic rock samples (+7.0 to +7.8‰) are explained by isotopic contamination of mafic magma by crustal material; indeed, mafic rock occurs as enclaves within acidic plutons, and U_2 granodiorite shows evidence of magmatic interaction giving rather low $\delta^{18}O$-values (+7.4 to +7.6‰). The nature of the interaction processes will be discussed in Section 7.4.

Table 3
The isotopic composition of Sr, Nd and O and concentrations of Rb, Sr, Sm and Nd in the Variscan calc-alkaline rocks (U_2) of Western Corsica and in the Variscan U_1 high-Mg–K granitoids and associated mafic rocks (age 322 ± 12 Ma)

Sample	Rb (ppm)	Sr (ppm)	$^{87}Rb/^{86}Sr$	$^{87}Sr/^{86}Sr$ ($\pm 2\sigma$)	Sm (ppm)	Nd (ppm)	$^{147}Sm/^{144}Nd$	$^{143}Nd/^{144}Nd$ ($\pm 2\sigma$)	$^{87}Sr/^{86}Sr$ t	ϵ_{Nd}^{t}	t_{DM}	$\delta^{18}O$ (‰ vs. SMOW)
VARISCAN CALC-ALKALINE ROCKS (U_2) OF WESTERN CORSICA:												
Granodiorites I (assumed age: 312 Ma):												
PR *7*	92.9	205	1.31	0.71277 (5)					0.70694			+7.6
PR *2*	110	220	1.45	0.71351 (6)					0.70705			+7.4
PR *3*	113	156	2.09	0.71609 (10)					0.70678			
PR *5*	155	170	2.65	0.71909 (4)					0.70729			
PR *4*	238	131	5.27	0.72918 (10)					0.70571			
Granodiorites II (assumed age: 312 Ma):												
CLB *32*	104	318	0.95	0.70944 (9)					0.70521			+7.4
CLB *12*	85.4	217	1.14	0.71272 (10)					0.70764			
CLB *23*	105	220	1.38	0.71340 (5)					0.70725			+8.0
CLB *28*	118	220	1.55	0.71394 (6)	8.4	40.0	0.1315	0.512295(10)	0.70704	−4.1	1,384	
CLB *25*	121	198	1.76	0.71496 (13)					0.70712			
CLB *10*	117	170	2.00	0.71574 (8)					0.70683			
CLB *21*	144	166	2.50	0.71713 (11)	5.6	28.0	0.1241	0.512359(20)	0.70599	−2.5	1,164	
CLB *31*	167	136	3.56	0.72202 (15)	4.7	23.8	0.1242	0.512308(15)	0.70616	−3.5	1,251	
PV *503*												+7.6
Monzogranites (age 312 ± 9 Ma):												
CLB *41*	68.7	226	0.88	0.71022 (7)	3.6	26.4	0.0855	0.512234(16)	0.70630	−3.4	967	+7.4
CLB *13*	90.9	191	1.38	0.71297 (8)					0.70682			
CLB *42*	94.3	190	1.44	0.71271 (9)	4.4	30.1	0.0917	0.512253(21)	0.70630	−3.3	991	
CLB *8*	89.8	135	1.92	0.71529 (13)					0.70674			
CLB *33*	103	110	2.71	0.71796 (10)					0.70589			
CLB *38*	130	127	2.96	0.71963 (9)	4.1	23.6	0.1089	0.512238(15)	0.70645	−4.3	1,171	
CLB *6*	151	102	4.27	0.72552 (6)					0.70650			+8.1
CLB *74*	160	100	4.63	0.72761 (11)					0.70699			
CLB *72*	144	77.0	5.41	0.73097 (9)					0.70687			
CLB *77*	181	91.1	5.76	0.73208 (10)	5.1	28.9	0.1107	0.512241(15)	0.70642	−4.3	1,187	+8.3
CLB *78*	183	90.4	5.86	0.73242 (8)					0.70632			
CLB *76*	179	79.2	6.54	0.73502 (9)					0.70589			

Leucocratic monzogranites (age 290 ± 6 Ma):

CLB *69*	188	90.1	6.06	0.73090 (8)	5.5	27.0	0.1277	0.512336(14)	0.70589	−3.3	1,252	
CLB *68*	215	88.4	7.05	0.73432 (8)	5.5	26.6	0.1296	0.512330(15)	0.70523	−3.5	1,290	
CLB *75*	271	47.1	16.5	0.77602 (10)					0.70793			
CLB *67*	213	36.0	17.3	0.77577 (10)	3.1	14.3	0.1359	0.512410(16)	0.70438	−2.2	1,239	+8.4
CLB *65*	291	25.6	33.4	0.84342 (5)					0.70560			
CLB *61*	311	23.7	38.6	0.86538(12)	6.5	24.6	0.1657	0.512362(16)	0.70610	−4.2	2,164	
CLB *62*	348	23.7	43.2	0.88096 (10)					0.70270			
CLB *63*	306	20.6	43.7	0.88522 (8)					0.70489			+8.9
CLB *55*												+8.5

Mafic suite (assumed age 280 Ma)[a]:

PC *6*	–	–	–	0.70397 (9)	1.33	3.27	0.2549	0.512768 (12)	0.70393	+0.5	–	
PC *4*	0.5	429	0.003	0.70478 (8)	0.82	4.01	0.1281	0.512732(19)	0.70477	+4.3	574	+6.5
PC *7*	0.5	388	0.004	0.70403 (11)					0.70401			
LM *169*	1.2	533	0.007	0.70430 (7)	0.56	3.31	0.1061	0.512645(47)	0.70427	+3.4	580	+5.1
CLB *24*	10.8	335	0.093	0.70521 (4)	4.05	16.6	0.1525	0.512635(35)	0.70484	+1.5	1,020	+5.9
CLB *20*	8.5	324	0.076	0.70737 (13)					0.70707			+6.4
CLB *18*	24.7	374	0.19	0.70796 (13)					0.70720			+6.2
PV *532*												+6.3
P *1*												+6.8
P *6*	1.5	490	0.009	0.70440 (8)					0.70436			+6.5
CLB *5*	89.0	232	1.11	0.71041 (11)	5.12	22.7	0.1415	0.512329 (29)	0.70599	−4.0	1,502	+7.2
CLB *7*	18.6	348	0.15	0.70659 (6)	3.43	15.9	0.1356	0.512362 (10)	0.70599	−3.2	1,326	
CLB *15*										+6.4		
CLB *40*	27.2	337	0.23	0.70802 (9)					0.70710			+6.7
CLB *43*	57.8	345	0.49	0.70853 (4)					0.70658			+7.0
CLB *27*	96.7	233	1.20	0.71272 (13)	6.33	33.1	0.1200	0.512296 (10)	0.70794	−3.9	1,215	+7.8
CLB *30*	84.3	301	0.81	0.71008 (9)					0.70685			+7.8
CLB *34*	38.9	451	0.25	0.70648 (12)	5.65	29.6	0.1198	0.512367(11)	0.70548	−2.5	1,100	+6.8

Table 3 (*continued*)

Sample	Rb (ppm)	Sr (ppm)	$^{87}Rb/^{86}Sr$	$^{87}Sr/^{86}Sr$ ($\pm 2\sigma$)	Sm (ppm)	Nd (ppm)	$^{147}Sm/^{144}Nd$	$^{143}Nd/^{144}Nd$ ($\pm 2\sigma$)	$^{87}Sr/^{86}Sr$ t	ϵ_{Nd}^{t}	t_{DM}	$\delta^{18}O$ (‰ vs. SMOW)
VARISCAN U_1 HIGH-Mg–K GRANITOIDS AND ASSOCIATED MAFIC ROCKS (AGE 322 ± 12 Ma):												
Monzodiorites–monzogranites:												
1	201	683	0.85	0.71090 (12)					0.70700			
3	170	569	0.87	0.71069 (7)	11.5	67.0	0.1076	0.512284(11)	0.70670	−3.3	1,092	
2	193	533	1.05	0.71143 (7)					0.70662			
K *24*	196	343	1.66	0.71406 (9)	4.2	23.1	0.1139	0.512308(15)	0.70645	−3.1	1,124	
4	179	308	1.68	0.71408 (5)					0.70638			
5	221	356	1.79	0.71454 (10)					0.70634			
8	204	344	1.72	0.71501 (10)					0.70713			
K *22*	231	304	2.20	0.71612 (5)	4.9	28.8	0.1066	0.512293(10)	0.70604	−3.1	1,070	+6.1
7	235	204	3.33	0.72139 (13)					0.70613			
6	222	192	3.35	0.72138 (9)					0.70603			
K *12*	239	192	3.61	0.72232 (5)	2.9	20.6	0.0882	0.512284(11)	0.70578	−2.5	927	+8.0
K *21*												+8.2
Syenomonzonites:												
K *1*												+5.9
K *5*	203	1,182	O.S0	0.70866 (10)	18.7	115.9	0.1011	0.512245 (9)	0.70637	−3.8	1,082	
K *6*	248	1,173	0.62	0.70877 (6)					0.70593	+6.4		
K *2*	159	1,067	0.43	0.70817 (7)					0.70620			+6.8
K *4*	288	1,242	0.67	0.70794 (10)	22.1	150.1	0.0923	0.512284(17)	0.70487	−2.7	958	
K *25*	197	1,401	0.41	0.70651 (12)	20.0	111.2	0.1127	0.512499(11)	0.70463	+0.7	830	
K *18*	165	515	0.93	0.71234 (7)	9.2	52.1	0.1107	0.512205 (8)	0.70808	−5.0	1,240	+5.9

Error in the $^{87}Sr/^{86}Sr$ measurements are better than $\pm 10^{-4}$. $\lambda^{87}Rb = 1.42 \cdot 10^{-11}$ yr^{-1}. Parameters used for calculation of Nd depleted mantle model ages and for ϵ_{Nd}^{t} are: $\lambda^{147}Sm = 0.654 \cdot 10^{-11}$ yr^{-1}; $(^{143}Nd/^{144}Nd)^{0}_{CHUR} = 0.512638$ (Jacobsen and Wasserburg, 1984); $(^{147}Sm/^{144}Nd)^{0}_{CHUR} = 0.196.7$ (Jacobsen and Wasserburg, 1984); t_{DM} has been calculated according to DePaolo (1981a, b).

[a]Peridotites: PC *6*; troctolites: PC *4*, PC *7*, LM *169*; gabbros: PV *532*, P *1*, P *6*, CLB *5*, *7*, *15*, *40*, *43*; diorites: CLB *27*, *30*, *34*.

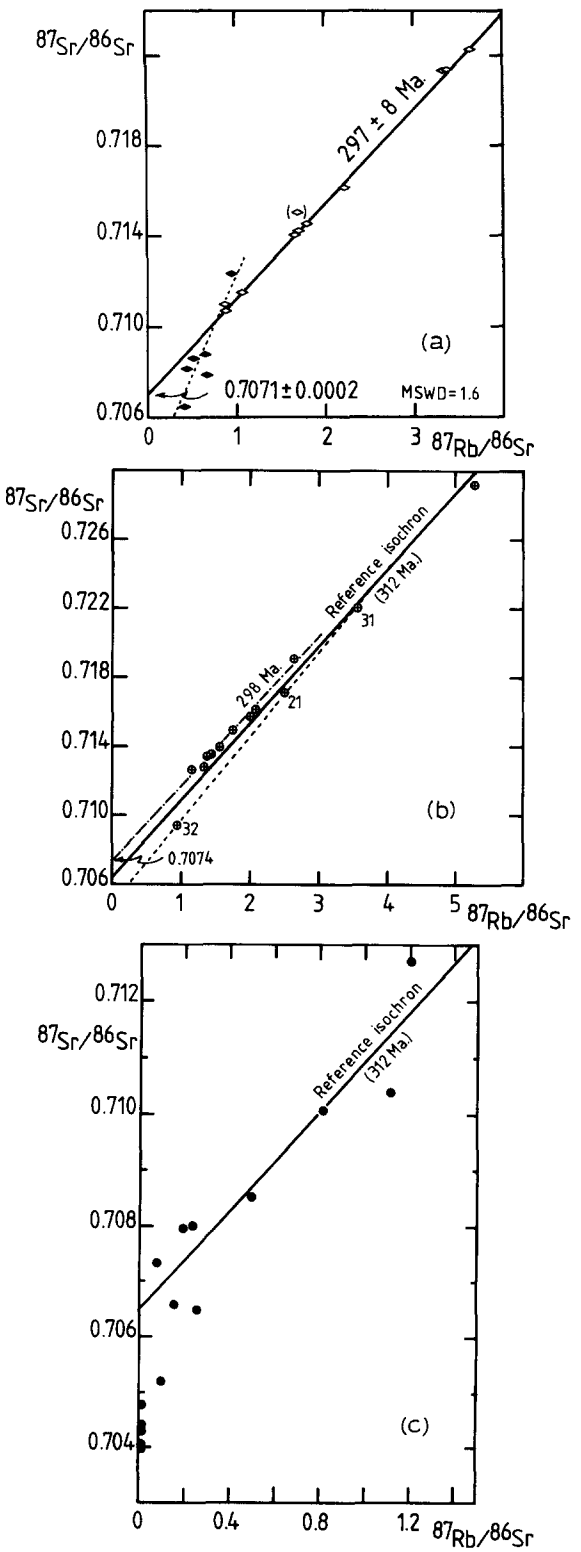

Fig. 7. $^{87}Sr/^{86}Sr$ vs. $^{87}Rb/^{86}Sr$ plots of Corsican Variscan granitoid rocks.

a. Rb–Sr isochron for the U_1 Mg–K suite, using only granite samples (*open diamonds*). Basic rocks (*solid diamonds*) do not define an isochron.

b. No isochron can be drawn for granodiorite of the U_2 association. Two groups of rocks are distinguished: one with a narrow range in variation of Rb/Sr ratios, defining a correlation line with an indicative age (298 Ma); the other, composed of three samples falling above the reference isochron (monzogranite: 312 Ma), could represent a mixing line (see text for discussion).

c. Distribution of basic rock of the U_2 association in the Rb–Sr diagram, compared to the monzogranite reference isochron (312 Ma).

Isochrons for U_2 granitoid rock are from Cocherie et al. (1992)

The U_1 Mg–K association does not show the same regular trend as the U_2 calc-alkaline composite association (Table 3); within U_1 the $\delta^{18}O$ of syenomonzonite ranges from +5.9 to +6.8‰, but the values for monzodiorite and monzogranite (+5.9 to +8.2‰) overlap with those of syenomonzonite. With the exception of contaminated and hybridized samples, the mafic rock in both U_1 and U_2 has low $\delta^{18}O$-values (U_2: +5.1 to +6.5‰; U_1: +5.9 to +6.8‰) that are typical of a mantle origin. Variscan mafic plutonic rocks from previous studies (Michard-Vitrac et al., 1980; Fourcade, 1981; Cocherie et al., 1994) show higher values for such rock. Similarly, the U_2 leucomonzogranite has a narrow range of $\delta^{18}O$-values (+8.4 to +8.9‰) that is significantly lower than that of Variscan two-mica granites (Michard-Vitrac et al., 1980). Fig. 10 shows different trends for Sr and O isotope data. Trend "*D*" (differentiation) may correspond to fractional crystallization of an acidic magma of monzogranitic composition (U_2) and trend "C.M." (contamination/mixing) mainly corresponds to U_2 mafic rock. Both trends show an increase of the initial Sr ratio as well as increasing $\delta^{18}O$-values, which indicates crustal contamination with possible assimilation during fractional crystallization of a mantle-derived magma (H.P. Taylor, 1980; H.P. Taylor and Sheppard, 1986) or direct acid–basic hybridization. This underlines the narrow range of variation in iso-

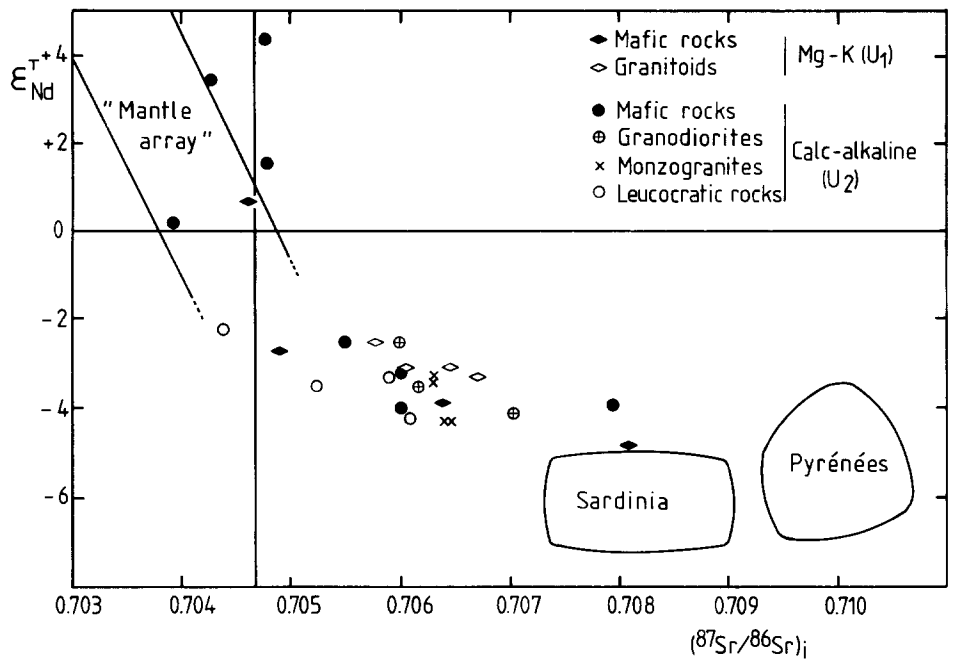

Fig. 8. $\epsilon_{Nd}(t)$ (ϵ_{Nd} at the assumed t age) against the initial $^{87}Sr/^{86}Sr$ ratio. Most points cluster round $\epsilon_{Nd}(t) = -3$ and $(^{87}Sr/^{86}Sr)_i = 0.706–0.707$. Five mafic rocks plot near the "mantle array". Despite assimilation and/or contamination, the corresponding magmas show a mantle origin. The $^{87}Sr/^{86}Sr$ ratio of the "bulk Earth" has been calculated at an age of 300 Ma, using a present-day Sr isotope composition of 0.70478 and a Rb/Sr ratio of 0.025. Pyrenean data are from Ben Othman et al. (1984) for the Quérigut and from Bickle et al. (1988) for the Trois Seigneurs plutons. Sardinian data are from Bouchet et al. (1992).

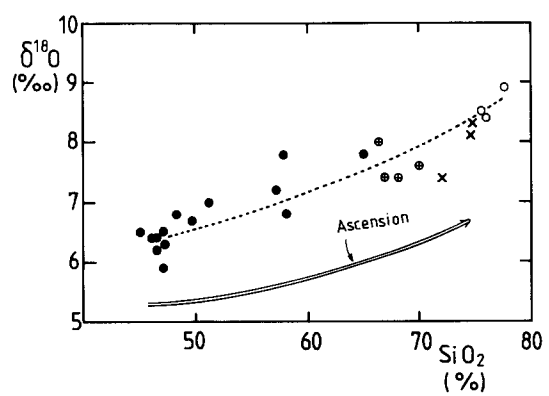

Fig. 9. Whole-rock $\delta^{18}O$-values vs. SiO_2 content for calc-alkaline rocks (U_2 association) from Corsica. The evolution trend of Ascension volcanic rocks is plotted for comparison (Weiss et al., 1987).

tope data for all rock types, and the contrasting values for Corsican and Pyrenean granitoid rocks (Michard-Vitrac et al., 1980). Thus, a large mantle contribution to mafic magma is much more evident for Corsica than for the Pyrénées, where the trend does not extrapolate to an end-member with mantle-type values (Sheppard, 1986).

Isotope data indicate that, in U_1 and U_2, the mafic rocks are mantle-derived and acidic rocks are crustal-derived from a source with the same isotope composition. Intermediate U_2 granodiorite could be the result of mixing processes. Thus, in the southern Variscan realm, a clear isotopic zonation appears from Corsica to the Pyrénées, whose origin will be discussed in a further section.

6. The U_1 Mg–K association

Let us consider, for the U_1 association, the genetic relationships between various magmas, the processes involved (see Appendix B), and the characteristics and origin of the primary liquids. Several questions arise concerning these comag-

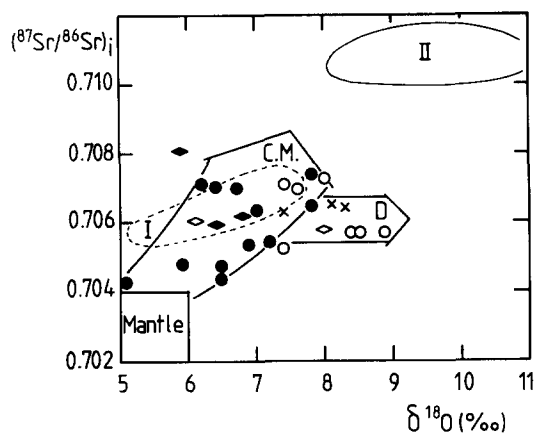

Fig. 10. Sr–O diagram for all analysed rocks (same *symbols* as in Fig. 8) The U_2 mafic suite indicates a mantle affinity, although a crustal contamination trend (*CM*) appears. The *large arrow* corresponds to the evolution of U_2 mafic rock from Corsica, showing a general trend of mixing–contamination from an initial magma of mantle origin. Note the narrow isotopic range of variation for the granite, with a weak increase of $\delta^{18}O$ for the most differentiated rocks (trend *D*). Fields *II* and *I* correspond to typical granite and associated mafic rock, respectively, from the Pyrénées (St. Laurent-la-Junquera; Cocherie, 1984).

matic acid and mafic rocks (Rossi and Cocherie, 1991):

(1) Do genetic links exist between all Mg–K rocks, as suggested by chemical mineral data but ruled out by isotope data?

(2) What, if any, is the magmatic process that can lead to the association of rocks described above?

(3) Is it possible to identify the source(s) of the initial magma and, if not, what are the end-members?

Major- and trace-element data indicate similar geochemical characteristics for all rocks of the Mg–K association, i.e. high Mg, Co, Cr and Ni concentrations, high contents of incompatible elements (K_2O, Rb, LREE, Th, U, Zr, Hf, etc.), and rather strong REE fractionation without large Eu anomalies. Decreasing REE contents correlate with increasing SiO_2 content. Mineral composition varies only slightly from mafic to felsic rock-types (Rossi, 1986; Laporte, 1987). All these facts point at a genetic link between all U_1 rocks, including the mafic ones. However, isotope data rule out such a genetic link:

(a) On the Rb–Sr isochron diagram, the ultra-K mafic rocks do not plot on the isochron line drawn using only the acidic rocks (Fig. 7a): the mafic rocks define a linear correlation that intersects the isochron; most representative points plot under the isochron, but one is located above it. This mafic correlation line can be interpreted as a mixing line between a mantle end-member and a crustal component that is distinct from the felsic Mg–K-suite protolith.

(b) Sm–Nd data lead to the same conclusion. The $\epsilon_{Nd}(t)$ of felsic rock has a narrow range of variation (-3.3 to -2.5) whereas the $\epsilon_{Nd}(t)$ of mafic rock ranges from -5.0 to $+0.7$, suggesting mixing between mantle-derived material and a crustal component, different from the crustal source of felsic magma.

(c) For two monzogranites the $\delta^{18}O$-values are $+8.0$ and $+8.2$‰. The lower $\delta^{18}O$-value ($+6.2$‰: sample K *22*) is thought to indicate isotopic disequilibrium, or a non-magmatic equilibrium temperature, but mineralogical studies point at an equilibrium. $\delta^{18}O$-values of Mg–K mafic rock are below $+6.8$‰; providing evidence for the non-cogenetic character of mafic and felsic rocks in the U_1 Mg–K association.

Isotope data distinguish at least two groups of samples on each side of the compositional gap seen in Harker's projections (Fig. 2). The gap for acid rock yields a Rb–Sr mixing line, whereas the other group, mainly composed of mafic rock, gives scattered isotope values. The Sr and Nd isotope characteristics of all U_1 Mg–K granites, ranging from monzodiorite (SiO_2 60%) to leucosyenogranite (SiO_2 75%) indicate a possible cogenetic suite, which will be tested by trace-element calculations.

6.1. U_1 *ultra-K mafic rocks*

The data points of mafic U_1 Mg–K rocks are scattered in both Rb–Sr-isochron (Fig. 7a) and Sr–Nd (Fig. 8) diagrams, suggesting a mixing process between two end-members consisting of mantle-derived material and a crustal component. According to isotope data, the crustal component appears to be ^{87}Sr-enriched and ^{143}Nd-depleted, compared to U_1 Mg–K granite. Thus,

the crustal end-member did not contribute to the magma that gave rise to the Mg–K acidic rocks. Additional evidence is provided by the REE pattern of sample K *18* (Fig. 4a), which appears to be the most contaminated sample with respect to Sr and Nd isotopes. Its REE fractionation is similar to that of normal detrital sedimentary rock (Wildeman and Haskin, 1973; Gromet et al., 1984), and different from that of Mg–K granite (Fig. 4b and c) which shows greater HREE fractionation.

The K_2O/Na_2O and the La/Yb ratios vary as a function of the importance of the crustal component, as shown on the Rb–Sr isochron (Fig. 7a); they decrease with increasing Sr_i and with decreasing $\epsilon_{Nd}(t)$. In other words, the high K_2O and LREE contents seem characteristic of a primary mantle-derived magma, but not of a crustal component. Foley et al. (1987) already suggested that magma mixing or assimilation of silica-rich crustal material is not the cause of K enrichment in igneous rocks. A spider-diagram plot of the U_1 ultra-K rocks identified them as lamprophyre (Fig. 11).

Foley et al. (1987) also questioned the origin of such highly potassic mantle-derived magmas; at present, several models have been proposed, including: a high degree of crystal fractionation (O'Hara and Yoder, 1967); zone refining (Harris, 1974; Neal and Davidson, 1989); an extremely small degree of partial melting of garnet–peridotite mantle material (Sun and Hanson, 1975; Jahn et al., 1979); fusion of a metasomatized mantle source (Mitchell and Bell, 1976; Hawkesworth and Vollmer, 1979; Wass and Rogers, 1980; Windom and Boettcher, 1980; Venturelli et al., 1984a, b; Mitchell et al., 1987); or leaching of wall rock and enrichment of incompatible elements during ascent of the melt (Alibert et al., 1983). Finally, McKenzie (1989) has proposed that melt fractions as small as 0.001% can separate from a 100-km-thick mantle layer; the metasomatized layer, in which small melt fractions accumulate, remelts at low temperature either through adiabatic decompression when crust is stretched, or through a temperature increase caused by a hot plume, giving strongly potassic magma.

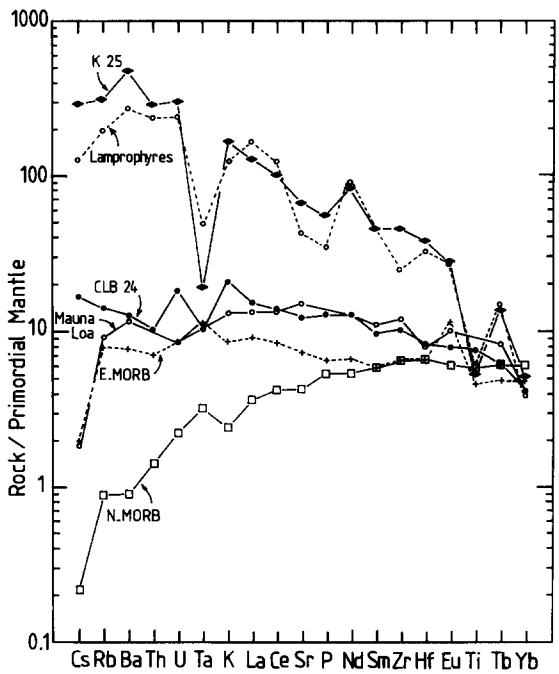

Fig. 11. Trace-element abundance in gabbro samples K *25* and CLB *24*, representative of primitive mafic magmas associated with U_1 and U_2 granite, respectively. Primitive mantle normalizing values are from Sun and McDonough (1989). The sequence of elements is based on the order of decreasing incompatibility in oceanic basalts. Data are compared to values for average N-MORB and E-MORB (Sun and McDonough, 1989), and average calc-alkaline lamprophyre estimated by Rock (1987).

In our opinion it is difficult to imagine that fluids can act as a carrier for various chemical elements, i.e. LREE, K, Rb, Cs, Zr, Hf, Th, U, Ta, Sr and Ba (Fig. 11). As proposed by Alibert et al. (1983), we consider that, if metasomatic fluids really are involved, their major role would be to favour the melting process without producing extensive change in the general chemistry of melt products. The production of ultra-K mafic rock from a zone-refining process fits well with trace-element and isotope data from Corsican U_1 mafic rocks. During the first hypothetical stage, a phlogopite(±garnet)-bearing source melts at ~200-km depth. The rising magma induces a zone-refining process in the traversed mantle, leading to a significant increase of incompatible-element contents, whereas the isotopic characteristics of the melt remain of mantle affinity,

despite the increase in Sr and Nd concentrations. In a second stage, this enriched magma interacts with the base of the crust, leading to lower La/Yb, higher $^{87}Sr/^{86}Sr$ and lower $^{143}Nd/^{144}Nd$ ratios. Interaction, i.e. contamination or assimilation during crystal fractionation, with the associated U_1 Mg–K felsic rock does not seem to be the major process involved.

6.3. Fractional crystallization of U_1 acidic rocks

A discussion of the relationships between Mg–K granites, using trace-element data, first needs identification of the magmatic process involved, after which the petrogenetic model (mineral proportions in equilibrium with liquid, rate of evolution of the magmatic process) is quantified, using trace-element and especially REE patterns. The last, in all Mg–K-granites, are strongly fractionated compared to calc-alkaline monzogranite (Figs. 4 and 5). As SiO_2 increases, ΣREE decreases from ~300 to 100 ppm, as do Sr and Ba contents, whereas the Eu anomaly is fairly constant ($Eu/Eu^* = 0.75$) as is the Rb content at around 200 ppm. Using log–log diagrams (Co vs. Th or Sr vs. Rb; Fig. 3a and b), it can be seen that compatible-element concentrations (Co, Sr) decrease sharply while incompatible elements (Th, Rb) increase only moderately. These data agree with fractional crystallization from a monzodioritic to a leucosyenogranitic magma, rather than magma mixing or partial melting. In Fig. 12, five REE (La, Sm, Eu, Tb, Yb), and Ba and Rb have been plotted against Sr on a log–log scale. Except for Yb, the correlations are fairly good, with an average correlation coefficient of 0.88. This provides additional evidence for fractional crystallization as the main process for explaining the geochemical trend from monzonitic to syenogranitic compositions. The correlations also indicate that distribution coefficients (D) remain constant, suggesting, as a first approximation, that the proportions of crystallizing solid phases are not greatly modified during magmatic evolution. Using simultaneous modelling of REE, Rb, Sr and Ba, we can test the fractional crystallization model for REE, after which we try to identify the mineral proportions of cumulate phases and calculate the extent of the fractional crystallization process.

Our calculated concentrations of Rb, Sr and Ba in the evolving liquid fit well with the analysed samples (heavy line in Fig. 12), using 11%, 50% and 24% for biotite, plagioclase and K-feldspar, respectively. On the other hand, it is well known that REE are also controlled by amphibole and accessory apatite, zircon, allanite, titanite, etc.; in our case we saw that titanite also plays an important role during crystallization. Calculated REE concentrations obtained with 12% of amphibole and 3% of titanite lead to REE patterns (Fig. 13) that are very similar to the experimental data of Fig. 4b and c. Initial concentrations in the primitive liquid of monzodioritic composition (L_0 in Table 4) were selected using the correlation diagrams of Fig. 12.

The trace-element content of the U_1 initial liquid of monzodioritic composition now has been well defined and, supported by isotope data, will be used to study the origin of primary acidic magmas.

6.4. Magma mixing in the U_1 association.

Summarizing the geochemical and mineral chemical data on U_1 rocks leads to a paradox: the existence of mafic–felsic interaction within the U_1 association, leading to a rock of intermediate composition, is supported by field evidence of mixing processes and by the occurrence of microgranular mafic enclaves of ultrapotassic composition in monzonite to monzogranodiorite. However, the isotope data suggest a gap between: (1) a mantle-derived ultrapotassic mafic magma; and (2) a felsic magma of crustal origin, showing no significant interaction with the mafic magma.

7. The U_2 calc-alkaline association

7.1. Mafic rock

About forty mafic samples belonging to the U_2 calc-alkaline association were collected in var-

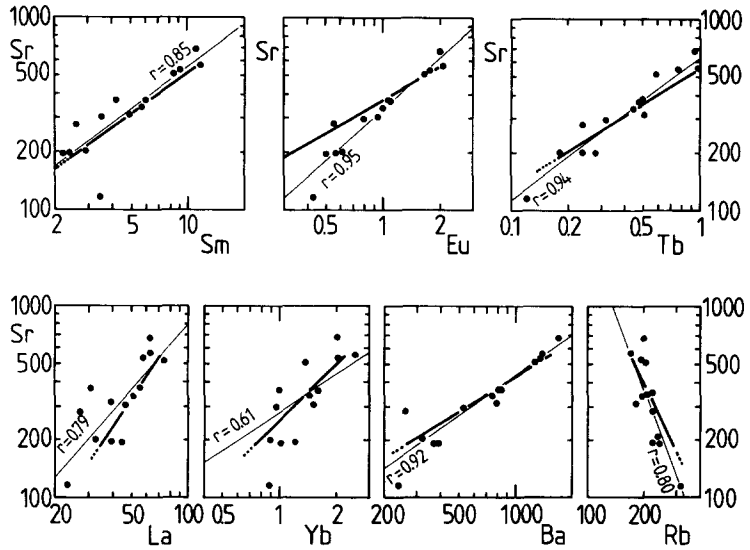

Fig. 12. Plots of REE, Rb and Ba against Sr on a log–log scale, for U_1 high-Mg–K granite. Calculated correlation lines (*fine lines*) are shown, suggesting a one-stage crystallization process. Note that only Rb behaves as an incompatible element, whereas all others decrease with increasing crystallization. The *heavy lines*, obtained from the calculated model (Table 4), fit well with the fine statistical lines.

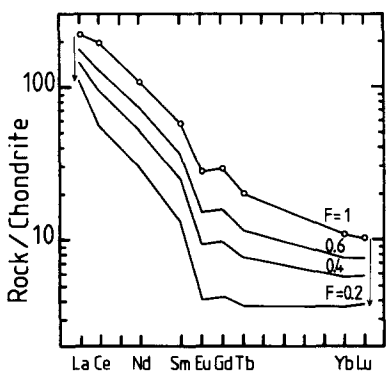

Fig. 13. Calculated REE patterns for U_1 Mg–K granite (Table 4). REE concentrations of the initial liquid (L_0 for $F=1$) have been graphically estimated with the log–log diagrams of Fig. 12.

ious locations (MUC of Pila Canale, Levie, Roccapina, Fozzano–Peloso; or smaller mafic septa). All samples were analysed for major and trace elements, and also REE (Cocherie, 1984; Cocherie et al., 1984), but at the time it was unclear whether there were several mantle or crustal sources. The inverse geochemical method (Appendix B), using trace-element data in log–log diagrams (Cocherie, 1986), has demonstrated that most of this variation can result from fractional crystallization, as the points representative of liquids fall near a straight line characteristic of such a process. Methods for graphic determination of bulk-distribution coefficients D for compatible (Cr, Ni) and incompatible or hygromagmatophile (U, Rb, Cs, Ta, Hf, Th, La) elements are described elsewhere (Allègre et al., 1977; Treuil et al., 1979; Cocherie, 1986), using the covariance between the fourteen possible pairs of elements. One MUC (Pila Canale) was selected for quantitative study because of its large size and wide variety of composition, ranging from troctolite to diorite and gabbro; ten of such samples plot on a straight line on a log Ni $=f($log Ta) diagram (Fig. 14). They range in composition from gabbro to diorite and show no cumulative textures; however, troctolite has cumulative textures and may be considered as a pure cumulate. Three samples plot close to the cumulative line (PC *4*, *532*, P *6*). Considering their texture and location in the diagram, we consider them as cumulates in equilibrium with fractionated to highly fractionated liquids. Other points (not plotted on Fig. 14) scattered between the cumulative and liquid-evolution lines are con-

Table 4
Trace-element model calculations, with fractional crystallization, using a primitive liquid of monzodioritic composition to produce the U_1 Mg–K association

	K_d					L_0	D	L_1 (F=0.6)	L_2 (F=0.4)	L_3 (F=0.2)
	plagio-clase	K-feld-spar	bio-tite	amphi-bole	tita-nite					
Rb	(0.048)	(0.34)	5.2	0.047	0.01	170	0.684	200	227	283
Sr	1.42	(3.87)	(0.12)	0.034	0.031	550	1.657	393	301	191
Ba	(0.36)	(6.12)	3.75	0.050	0.019	1500	2.073	867	561	267
La	0.43	0.05[a]	0.051	1.43	34.1	70	1.427	56.3	47.3	35.2
Ce	0.30	(0.044)	0.034	1.95	46.6	160	1.796	107	77.1	44.4
Nd	0.15	(0.025)	0.031	2.90	46.0	65	1.812	42.9	30.9	17.6
Sm	0.14	(0.018)	0.029	3.95	45.5	11	1.917	6.89	4.75	2.52
Eu	0.69	(1.13)	0.022	2.05	44.1	2	2.188	1.09	0.67	0.30
Gd	0.12	(0.011)	0.031	6.38	45.0	7.5	2.182	4.10	2.54	1.12
Tb	0.11	0.011[a]	0.024	5.10	45.9	1	2.049	0.59	0.38	0.19
Yb	0.06	(0.012)	0.036	4.71	35.5	2.2	1.667	1.57	1.19	0.75
Lu	0.07	(0.006)	0.038	4.89	33.0	0.33	1.617	0.24	0.19	0.12

K_d=individual partition coefficients for the studied elements were empirically determined by measuring of concentrations in separated biotites, amphiboles and plagioclases, as well as concentrations in whole rocks. A calc-alkaline granitoid association was used, ranging in composition from diorite to granodiorite (Cocherie, 1984). Values in brackets are from Arth (1976). D=calculated bulk distribution coefficients using the respective proportions of crystallizing minerals: plagioclase (50%), K-feldspar (24%), biotite (11%), amphibole (12%) and titanite (3%). L_0=initial concentration in primitive monzodiorite, inferred from correlation diagrams of Fig. 12. L_1, L_2, L_3=calculated liquid concentrations according to the Rayleigh distillation law ($L_n/L_0=F^{D-1}$), for F=0.6, 0.4 and 0.2, respectively. These concentrations can be compared with the sample concentrations listed in Table 1.
[a]Extrapolated values.

sidered as mixing of melt and cumulate. Accessory minerals, e.g., chromite, can play a major role in Cr and Ni concentration. This role is taken into consideration by the inverse geochemical approach without any hypothesis on bulk-distribution coefficients and phases in equilibrium with the liquid. Knowledge of the bulk D-values for U, Rb, Cs, La, Th, Ta, Hf, Ni and Cr, as well as their concentrations in less (CLB *24*) and more differentiated melts, enables calculation of the degree of fractional crystallization. In this example, the mean of nine calculated F-values is 0.17 ± 0.08, which corresponds to a high degree of crystallization of $83 \pm 8\%$. This means that the cumulates remained in equilibrium with the evolving melt and that the liquids in question are cogenetic. The initial melt is thus clearly identified.

A test of this model is based on conventional REE systematics. REE concentrations of the various possible melts are calculated by using the previously determined fractional-crystallization model (Rayleigh distillation law) and the known REE contents (Fig. 6a) of the identified pure cumulates (Fig. 14). This identifies the REE content of the initial liquid and evaluates its degree of fractional crystallization, in order to compare it to the value calculated with log–log diagrams. Note that such calculations do not require a knowledge of partition coefficients, as the analysed cumulates are assumed to be representative of the instantaneous solid phases in equilibrium with the evolving liquids. According to Fig. 14, three kinds of cumulates can be distinguished: troctolite (with very low hygromagmatophile-element contents and transition-element enrichment), gabbro-norite, and gabbro (with lower transition-metal contents). One representative sample of each of the different cumulates has been selected (S*1*=PC *4*, S*2*=*532* and S*3*=P

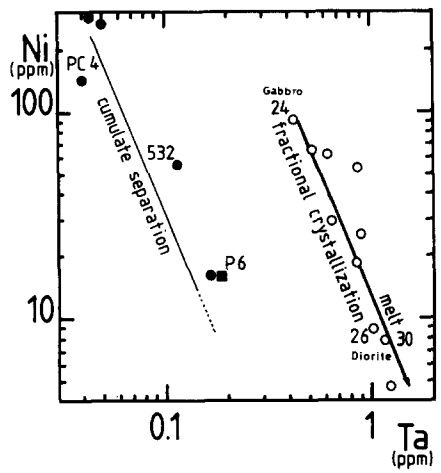

Fig. 14. Logarithmic plot of Ni against Ta of basic rock associated with the U_2 association in the Variscan batholith of Corsica. Two trends can be seen: *open symbols* correspond to rock representative of a melt (the Pila Canale is taken as an example); *solid symbols* represent cumulates. Many cumulate rocks plot between the two trends, as they are composed of cumulate minerals and interstitial minerals representative of the melt in equilibrium. PC *4*=troctolite; *532*=gabbro-norite; P *6*, CLB *24*=gabbros; CLB *30*=diorite.

6, respectively). The corresponding REE patterns are plotted in Fig. 6a. A three-stage fractional-crystallization model according to the Rayleigh law is summarized in Table 5.

The resulting bulk value F of the most evolved liquid L*3*=CLB *30* is: $F=F_1F_2F_3=0.70\times0.50\times0.70=0.24$, which corresponds to a crystallization index of 76%.

Table 6 lists the detailed calculations. The calculated initial liquid L_0 fits particularly well with the composition of a gabbro (such as CLB *24*), considered by Rossi (1986) as a possible initial melt on the basis of field and petrological data. The calculated crystallization index of 76% is close to the value of 83% previously determined from other trace elements using the inverse approach (see above).

REE calculations and the log–log diagram demonstrate that the U_2 mafic rock can be regarded as suite that evolved according to a fractional-crystallization process. Sr and Nd isotopes, however, show heterogeneous values of $(^{87}Sr/^{86}Sr)_i=0.7039–0.7079$ and $\epsilon_{Nd}(t)=-4.0$ to $+4.3$, from gabbro or troctolite to diorite (Figs. 7c and 8). This could suggest an assimilation/fractional-crystallization process (AFC), but the REE content of diorite (e.g., CLB *30*) is too high compared to that of granite (Figs. 5 and 6) to be considered as a result of such an AFC process. Similarly, Sr_i is higher and ϵ_{Nd} lower than that of granite.

So, if an AFC process is involved, the assimilated material did not derive from the associated granite magma. We think that crustal fluids interacted with the mafic magma during fractional crystallization. Thus, the first solidified liquid (gabbro) and the primitive cumulate (troctolite) have almost retained their primitive isotopic character, but the most evolved magma (diorite) interacted during a much longer period with crustal fluids. Nevertheless, this kind of interaction does not seem to have disturbed major- and trace-element geochemistry.

7.2. *Origin of* U_2 *mafic rocks*

The points of interest for mafic rock of the U_2 calc-alkaline association are: its origin, the nature of its source material, the degree of homogeneity of such source material and, if possible, the tectonic environment during the time of magma emplacement.

Table 5
Scheme for three-stage fractional-crystallization model

Liquid	$L_0\longrightarrow$	$L_1\longrightarrow$	$L_2\longrightarrow$	L_3 (diorite CLB *30*)
	$D_1=S_1/L_1$	$D_2=S_2/L_2$	$D_3=S_3/L_3$	
	$F_1=0.70$	$F_2=0.50$	$F_3=0.70$	
Cumulates	S_1 (PC *4*)	S_2 (*532*)	S_3 (P *6*)	
	Troctolite	Gabbro-norite	Gabbro	

Table 6
REE calculated for liquids (L_2, L_1, L_0) of the U_2 mafic suite, according to a fractional crystallization model

	L_3 CLB *30*	S_3 P *6*	D_3	L_2 (F_3=0.7)	S_2 *532*	D_2	L_1 (F_2=0.5)	S_1 PC *4*	D_1	L_0 (F_1=0.7)	CLB *24*
La	38.1	10.4	0.273	29.4	5.23	0.178	16.6	1.5	0.090	12.0	10.5
Ce	77.7	24.8	0.319	60.9	10.4	0.171	34.3	3.8	0.110	35.0	24.4
Nd	40.8	18.0	0.441	33.4	(6.03)	0.181	18.9	(2.5)	0.132	13.9	17.5
Sm	9.00	5.45	0.606	7.82	1.53	0.196	4.48	0.71	0.158	3.32	4.30
Eu	1.90	2.73	1.437	2.22	0.58	0.261	1.33	0.46	0.346	1.05	1.33
Gd	8.10	5.67	0.700	7.28	(1.54)	0.212	4.22	(0.67)	0.159	3.13	4.00
Tb	1.25	0.93	0.744	1.14	0.25	0.219	0.66	0.11	0.167	0.49	0.67
Yb	3.81	2.32	0.609	3.31	0.90	0.272	2.00	0.43	0.215	1.51	2.07
Lu	0.61	0.31	0.508	0.51	(0.15)	0.294	0.313	0.070	0.224	0.24	0.31

The calculated L_0-values are compared to the analysed rock CLB *24* (see text for explanations). Interpolated values are in brackets

Table 7
Trace-element calculations using a non-modal batch partial melting model (Shaw, 1970) to produce mantle-derived liquids corresponding to the U_2 mafic suite

	K_d					Mauna Loa 1975 flow	L_0 CLB *24*	Amphibole lherzolite (F=0.1) S_1	Spinel lherzolite (F=0.1) S_2	Mantle (Shaw, 1980)
	olivine	clinopyroxene	orthopyroxene	amphibole	spinel					
Rb	0.010	0.022	0.031	0.29	–	5.8	9.0	1.2	1.0	0.945
Sr	0.014	0.017	0.12	0.46	–	319	262	38	34	39
Ba	0.010	0.013	0.026	0.42	–	81.4	89	11	9.9	7.1
La	(0.0066)	(0.018)	(0.08)	(0.10)	(0.03)	9.17	10.5	1.27	1.25	1.22
Ce	0.0069	0.024	0.15	0.20	0.03	23.6	24.4	3.31	3.17	4.24
Nd	0.0066	0.033	0.31	0.33	0.04	17.2	17.5	2.86	2.71	2.89
Sm	0.0066	0.054	0.50	0.52	0.05	4.86	4.30	0.86	0.80	0.919
Eu	0.0068	0.054	0.51	0.59	0.055	1.69	1.33	0.27	0.25	0.385
Gd	0.0077	0.091	0.61	0.63	0.07	5.46	4.00	0.90	0.84	–
Tb	(0.008)	(0.12)	(0.65)	(0.63)	(0.09)	–	0.67	0.16	0.15	–
Yb	0.014	0.34	0.62	0.49	0.11	2.08	2.07	0.56	0.52	1.065
Lu	0.016	0.42	0.56	0.43	0.09	0.305	0.31	0.083	0.083	0.164

K_d=partition coefficients from Arth (1976) except extrapolated values (in brackets) and those concerning spinel from Kay and Gast (1973). Mauna Loa=basalt from 1975 Hawaii flow (Newsom et al., 1986). CLB *24*=sample from Corsican U_2 mafic suite representative of primitive liquid. S_1=calculated trace-element concentrations in a mantle containing amphibole (Ol, 55%; Opx, 20%; Cpx, 15%; Amph, 10%); the solid phases involved in the melt are: Opx 20% and Amph 60%. S_2=calculated trace-element concentrations in a mantle containing spinel (Ol, 58%; Opx, 20%; Cpx, 20%; Sp 2%); the solid phases contributing to the melt are: Opx 45% and Cpx 55%. Mantle concentrations from Shaw (1980) are taken as reference.

As shown before, the Sr–Nd–O-isotope data of some mafic rocks clearly indicate a juvenile origin at the time of the batholith formation, i.e. $(^{87}Sr/^{86}Sr)_i$=0.704, $\epsilon_{Nd}(t)$=+0.2 to +4.6. Similarly, in the $^{87}Sr/^{86}Sr$ (age corrected) vs. $\epsilon_{Nd}(t)$ diagram, the less contaminated mafic samples plot not far from the mantle reference field (Fig. 8). From an isotopic point of view it is impossible to choose between juvenile lower-crustal material and direct partial melting of the mantle as possible sources. The first alternative can be rejected if we consider trace-element data

Table 8
Fractional crystallization model for U_2 calculated trace-element composition in primitive liquids of monzogranitic composition

	K_d			L_0 CLB *13*	D_1	L_1	C_1	D_2	L_2	C_2
	plagio-clase	K-feld-spar	mona-zite		(F_1=0.6)			(F_2=0.4)		
Rb	0.041	0.34	–	91	0.116	143	158	0.161	309	314
Sr	2.84	3.87	–	190	3.098	65	79	3.252	8	23
Ba	0.308	6.12	–	647	1.761	439	453	2.633	98	128
La	(0.30)	(0.06)	5,260	38.4	1.450	30.5	32.6	1.414	20.9	18.8
Ce	0.27	0.044	5,060	69.3	1.377	57.2	60.3	1.343	41.8	39.7
Nd	0.21	0.025	(4,500)	24.2	1.199	22.0	–	1.171	18.8	–
Sm	0.13	0.018	3,830	4.18	0.983	4.22	4.63	0.966	4.35	4.8
Eu	2.15	1.13	482	0.87	2.006	0.52	0.67	1.853	0.24	0.33
Gd	0.097	0.011	(1,750)	3.18	0.478	4.15	–	0.465	6.78	–
Tb	(0.08)	(0.008)	1,210	0.51	0.340	0.71	0.58	0.330	1.32	1.0
Yb	0.049	(0.006)	173	1.83	0.078	2.93	2.33	0.072	6.86	5.3
Lu	0.046	0.006	(115)	0.33	0.063	0.53	–	0.057	1.26	–

K_d=partition coefficients, those for plagioclase and K-feldspar are taken from Arth (1976), those for monazite correspond to the ratio of analysed monazites found in the leucocratic monzogranites (La, 9.89%; Ce, 20.1%; Sm, 1.84%; Eu, 159 ppm; Tb, 1210 ppm; Yb, 915 ppm) and the average content of ten whole rocks. Values in brackets are extrapolated.
L_0 CLB *13*=analysed monzogranite taken as the primitive monzogranitic liquid. D_1=calculated bulk distribution coefficients using the respective proportions of crystallizing minerals: plagioclase (75%), K-feldspar (25%) and monazite (0.023%). D_2=calculated bulk distribution coefficients using the respective proportions of crystallizing minerals: plagioclase (60%), K-feldspar (40%) and monazite (0.023%). L_1 and L_2 are the two corresponding liquids calculated according to the Rayleigh distillation law ($L_1/L_0=F^{P_{1-1}}$), using the calculated distribution coefficients, and with $F_1=0.6$ and $F_2=0.4$. This two-stage model leads to a bulk crystallization index of 76% ($F=0.24$). The L_1 and L_2 calculated concentrations fit well with the average concentrations C_1 and C_2 measured on differentiated monzogranites (7 samples) and leucocratic monzogranites (10 samples), respectively (Figs. 15 and 5b, respec.).

of the initial liquid (e.g., CLB *24*), i.e. its low Rb content (9 ppm) and the low REE contents (Figs. 6b and 11) with a slightly fractionated REE pattern from La to Lu (30× chondrite to 10× chondrite); a two-stage model involving partial melting of the mantle, followed by a second partial melting of this now solidified melt, would give much higher incompatible-element concentrations.

Several types of peridotite mantle source can be considered. The partial melting of garnet-lherzolite can easily be rejected, in view of the experimentally determined REE patterns of initial liquids (Fig. 6b) and the calculated pattern of the initial liquid (Table 6), because a garnet residue of partial melting would lead to liquids with HREE-depleted patterns. Furthermore, experimental work by Green (1980) showed that tholeiitic basalt cannot be formed in equilibrium with residual garnet. Two other mantle-source assemblages are more likely to give a liquid of tholeiitic or calc-alkaline composition, i.e. amphibole lherzolite and spinel lherzolite. The CLB *24* gabbro is taken as representative of "primary liquid" (Fig. 6b). Both types of source assemblage were tested, to calculate the REE, Rb, Sr and Ba contents (Table 7) of a possible mantle, instead of assuming a 2–3× chondritic abundance for trace elements in the mantle and calculating the possible primary magma. Both melting of amphibole lherzolite and of spinel lherzolite are appropriate, in that their calculation of trace-element concentrations leads to rather flat REE patterns (~3–4× chondrite), and Rb, Sr and Ba values that are compatible with mantle material (Shaw, 1980). This means that trace-element data alone do not suffice for choosing between these two mantle source assemblages. The large variation in HREE contents of the three samples plotted in Fig. 5b is

considered to be caused by mantle heterogeneity for HREE.

Using geochemical data, we can compare the U_2 mafic rocks with present-day or recent volcanism. They resemble tholeiitic island-arc basalt, e.g., from the Western Sunda volcanic arc of Indonesia (Nicholls et al., 1980): the K_2O contents are very similar (0.5–0.7%), but REE patterns are flatter in island-arc rocks than in our case. The Th/Ta ratio, another useful geochemical tool, remains constant during magmatic fusion and crystallization, as these two incompatible elements have similar behaviour. This ratio can thus be used to characterize both source materials and tectonic environment of the magmatic process (Joron and Treuil, 1977). Gabbro identified as "primary liquid" (e.g., CLB *24*), has a low Th/Ta ratio (2.1), which is typical of extensional tectonic areas, e.g., spreading ridges or intra-plate magmatism. However, higher Th/Ta ratios of >6 are thought to be related to convergent-plate tectonic environments, e.g., subduction zones. Shibata et al. (1979) studied tholeiitic basalt dredged from the Mid-Atlantic Ridge at 43°N that is very similar to our basic rocks. Their tholeiitic basalt is also enriched in incompatible trace elements, compared to tholeiitic mid-ocean ridge basalt (MORB), and is associated with alkali olivine basalt. Both are regarded as the result of vertical heterogeneities in mantle composition. Tholeiitic ocean-island basalt from the 1975 eruption of Mauna Loa in Hawaii (Table 8) shows the same incompatible-element abundances (Newsom et al., 1986). According to the Th–Hf–Ta diagram of Wood et al. (1979), U_2 mafic rock may be analogous to enriched MORB.

In summary, the data indicate the absence of a subduction zone in the tectonic environment of U_2 mafic plutonism, which agrees with palinspastic reconstructions (e.g., Vai, 1989). The rock of tholeiitic composition, enriched in incompatible elements with regard to ocean-floor basalt, can be compared to E-type MORB (Fig. 11) or ocean-island basalt, produced by nonmodal partial melting of a heterogeneous mantle of spinel or amphibole peridotite without garnet, i.e. under conditions of asthenospheric ascent.

7.3. U_2 monzogranite and leucomonzogranite

U_2 granitic rocks, in contrast with the mafic suite, show no characteristic trend in log–log diagrams. Several explanations are possible: (1) The various granite bodies are not genetically linked, even though isotope data indicate a cogenetic relationship; (2) differentiation, due to an unidentified magmatic process, is rather poor and interelement diagrams show clustering of representative points, although the isochron indicates a rather large interval of variation; (3) REE, U, Th, Ta, Rb, Cs, etc., are much less incompatible in acidic melts than in basic ones, which means that *D*-values approach or exceed 1, and compatible elements (Cr, Ni, Co, Sc, etc.) also have *D*-values close to 1. Thus, even with a high degree of differentiation and regardless of the magmatic process, the variations in concentration will be slight.

Nevertheless, several geochemical arguments indicate that monzogranite and leucomonzogranite derived from the same source:

(1) Using the log–log diagrams, e.g., log $Sr = f(\log Rb)$ (Fig. 3b), a general negative trend is observed, with strongly decreasing compatible-element contents associated with a rather moderate increase of incompatible-element contents. This is a typical variation trend for such element pairs during fractional crystallization of a magmatic suite.

(2) The homogeneous Sr and Nd isotope data: Sr_i 0.706–0.707; $\epsilon_{Nd}(t) = -4.3$ to -2.2 and the $\delta^{18}O$-values that increase from +8 to +9‰ are acceptable for a suite of rocks related through a high degrees of fractional crystallization (Le Bel et al., 1985; H.P. Taylor and Sheppard, 1986; Weiss et al., 1987).

(3) The degree of REE fractionation (Fig. 5b) varies from highly LREE-enriched patterns without Eu anomalies for rock with 70–72% SiO_2 (e.g., CLB *13*), to leucomonzogranite (SiO_2 75–77%) with flat normalized patterns and huge negative Eu anomalies.

The decrease of Sr and Eu concentrations related to an increasing SiO_2 content, suggests an important role of feldspar during magmatic differentiation of the initial monzogranitic melt.

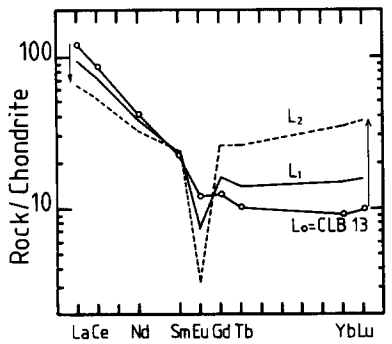

Fig. 15. Calculated REE patterns for U_2 calc-alkaline granite. A two-stage fractional crystallization model (Table 8) involving feldspar and monazite fits well with the data (Fig. 5b).

The decrease of Ba associated with increasing concentration of Rb and Cs, implies the crystallization of K-feldspar without mica. The large increase of HREE concentrations (Fig. 5b) also needs quartz crystallization in order to reduce the HREE bulk distribution coefficients. Thus, the primitive monzogranitic melt would appear to have had a composition close to that of granite. Crystallization of the major phases Qz, Pl and K-fs was not sufficient to account for the LREE decrease; therefore, we must consider that accessory LREE-enriched phases (allanite, monazite, etc.) accompanied the major phases. Such accessories act as a trap for LREE, leading to a decreasing LREE content with increasing crystallization index (Fourcade and Allègre, 1981; Miller and Mittlefehldt, 1982; Gromet and Silver, 1983). A two-stage fractional crystallization model involving Rb, Sr, Ba and REE concentrations is used to compare the calculated concentrations of residual liquids with the observed concentrations in calc-alkaline granite. The direct calculation method used for our work needs estimates of the following parameters (Table 8): (1) Monzogranite selected as primitive liquid (e.g., CLB *13*) shows the lowest SiO_2 content and the weakest negative Eu anomaly (Fig. 5b) compared with other monzogranites; and (2) in order to calculate bulk distribution coefficients, individual partition coefficients are needed for each mineral involved in magmatic differentiation (Table 8). It can be seen that the calculated liquid concentrations obtained at the first stage (L_1) are close to average concentrations (C_1: 7 samples) of the most differentiated monzogranites, i.e. increase of Rb and HREE, and decrease of Sr, Ba, Eu and LREE, compared to primitive monzogranite (Fig. 15). The second stage leading to the leucocratic liquid L_2 is compared to the average of leucocratic monzogranite (C_2: 10 samples). The previous trend of trace-element contents is confirmed by calculated REE patterns (Fig. 15).

The monzogranite–leucomonzogranite association can be considered as a suite, which evolved according to a fractional-crystallization model from an initial liquid of monzogranitic composition.

7.4. U_2 granodiorite as by-product of magma mixing

Deciphering the origin of rocks of intermediate composition, i.e. granodiorite, bridging the gap between mafic and acidic end-members, is crucial for interpreting the genesis of any calc-alkaline association. Isotope data from U_2 mafic rocks show an origin that is mainly mantle-derived magma and acidic crustal-derived material. The existence of a statistical gap from 60% to 65% SiO_2 in U_2 trends (Fig. 2), corresponding to granodioritic composition, emphasizes the key place of such rocks in the interpretation of a plutonic association. Acidic–mafic mingling zones in granodiorite were observed in the field in Corsica (Orsini, 1980; Rossi, 1986) whereas mingling and mixing were studied in Sardinia by Zorpi et al. (1991), who concluded that the origin of microgranular mafic enclaves in granodiorite must be sought in mixing between mafic and silicic magmas. As discussed before, such a suite of rocks of intermediate composition is characterized by strong geochemical heterogeneity. It is essential that nature and origin of the mixing batches are defined as accurately as possible, in order to place constraints on the genesis of rocks of intermediate composition in the U_2

association. The Corsican example is well suited for this purpose because of good exposures of both monzogranite and mafic rock, which permit detailed investigations into the nature of possible an end-members.

The use of trace-element log–log diagrams (e.g., Co/Th, Sr/Rb) when looking for relationships between monzogranite and granodiorite, is ruled out by the tight clustering of representative points. In a $^{87}Sr/^{86}Sr$ vs. $^{87}Rb/^{86}Sr$ diagram, the granodiorite points do not fit along a single isochron line (Fig. 7b). Nevertheless, two groups of rocks can be distinguished: (1) a first group roughly plots above the reference isochron of monzogranite, with slightly higher model Sr initial ratios (0.7074 instead of 0.7065); and (2) the second group of three rocks (i.e. CLB *32*, *21*, *31*) plots on a straight line with a much lower Sr initial ratio and an older age, which is inconsistent with field relationships. The first trend, defined by granodiorite with representative points close to the monzogranite isochron, has high SiO_2 and trace-element contents, e.g., REE of CLB *10*, PR*7* (Fig. 5a), which make them not so different from the primitive monzogranitic liquid. Both shape (no Eu anomaly) and level of REE abundance are similar to those of less differentiated monzogranite (CLB *13*). The second group has less acidic geochemical characteristics and specific REE patterns, e.g., CLB *21* (Fig. 5a); it shows higher HREE contents and a pronounced negative Eu anomaly, typical of highly differentiated rocks. The major-, trace-element and Sr isotope features together, provide a picture that is inconsistent with a direct common origin for these two groups of granodiorite. The second group, with its older "age" and a low model Sr initial ratio (Fig. 7b), may be interpreted as a result of mixing between mafic and silicic end-members.

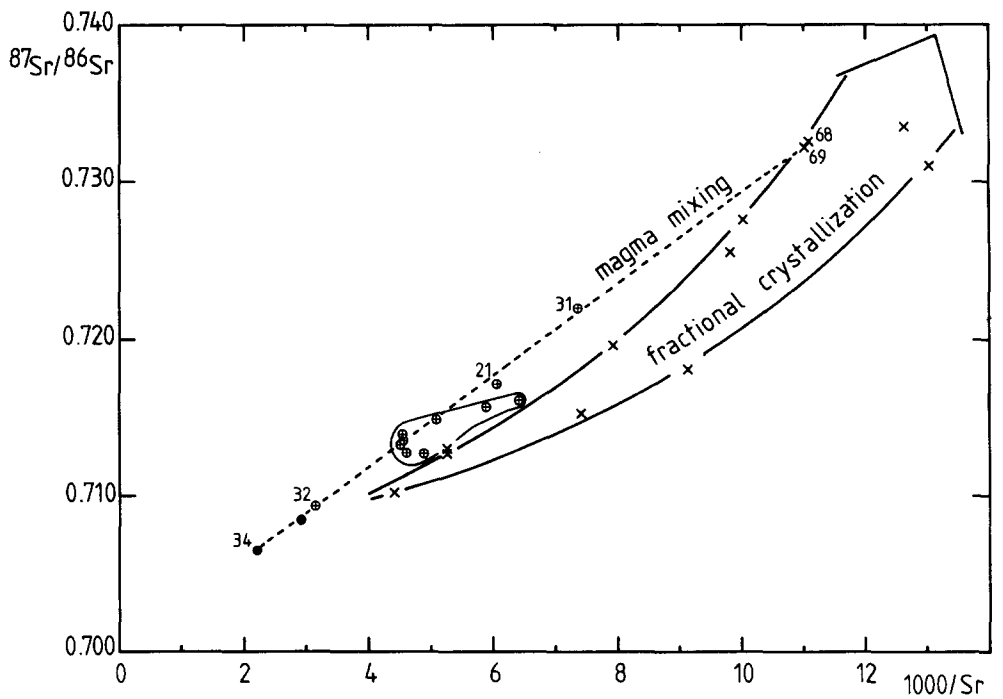

Fig. 16. $^{87}Sr/^{86}Sr$ vs. 1000/Sr plot for the U_2 calc-alkaline association (same *symbols* as in Fig. 8). Two groups of rocks of granodioritic composition appear. One group, represented mainly by samples *32*, *21* and *31*, plots along a mixing line between two end-members (differentiated basic rock and the crystallizing monzogranitic melt), leading to a mixing pseudo-isochron (Fig. 7b). The second group consists of samples clustered near the less differentiated monzogranite, defining a fractional crystallization trend in agreement with the calculated isochron at 312 Ma.

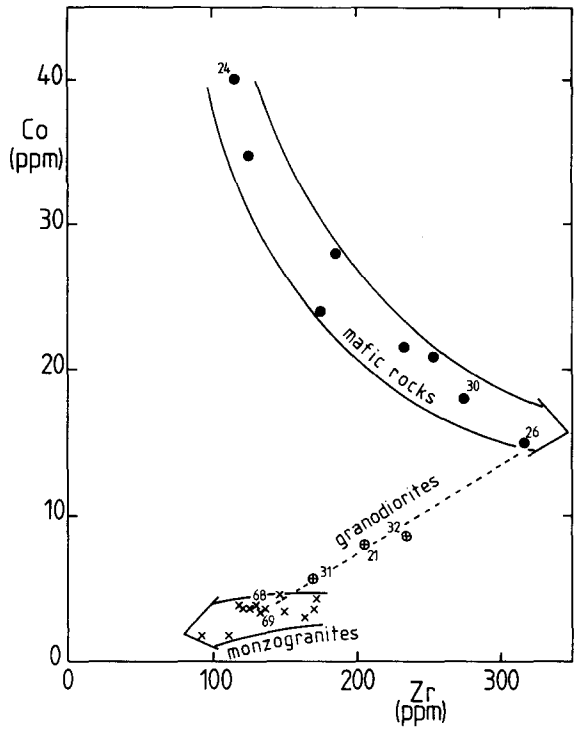

Fig. 17. Plot of Co against Zr for the U_2 association, showing the mixing trend of some granodiorite with monzogranite and highly differentiated magmas.

To test such a hypothesis and when the Sr initial ratios of the end-members are not very far apart, we prefer to use the $^{87}Sr/^{86}Sr$ (present-day) vs. 1/Sr diagram, which yields a mixing line when samples are linked by a mixing process (Bernard-Griffiths, 1975; Scharbert, 1992). This provides a curve for a suite of rocks evolving by differentiation (Fig. 16). We must emphasize that this test cannot be used if the Rb content remains constant for the entire rock suite, in which case this plot will be a mathematically straight line. In our case, the Rb concentrations increase according to the sequence from dioritic to monzogranitic, e.g., CLB *34*, *32*, *21*, *31*, *77* and *78* (Table 3). Fig. 16 shows how the representative points of the second group of granodiorites (e.g., CLB *32*, *21*, *31*), yielding a pseudo-isochron (Fig. 7b), give a mixing line between two end-members, the narrow field of mafic rocks and that of differentiated monzogranitic magma, corresponding to the highest Rb/Sr ratios of the isochron. Note, that the representative points of the first granodiorite group define a small field close to the beginning of the fractional-crystallization trend of monzogranite (Fig. 16), confirming the great similarity between this group of granodiorites and the less differentiated monzogranite. Another test involving a simple binary diagram can be used, requiring only those elements that show large variations in concentration; in this case, the mixing of two magmas leads to a straight line, whereas various different types of curve may be obtained according to the particular magmatic process involved. Such variation diagrams, using Co/Ba or Co/Zr (Fig. 17), show that granodioritic magma is the result of a mixing process between the most differentiated melts of the associated mafic suite, and the monzogranitic magma at the end of its first differentiation stage, before the leucomonzogranitic stage.

Field and structural considerations indicate that the two granodiorite groups could not have been different intrusive units: they have comparable chemical mineral composition with similar styles of textural disequilibrium and both groups contain microgranular mafic enclaves, interpreted as quenched inclusions of mafic magma that suffered extensive disaggregation and re-equilibration. The first group, which plots close to the monzogranite reference isochron (Fig. 7b), shows slight contamination by mafic magma, but has acquired isotopic homogeneity and plots in a field of trace-element composition close to that of monzogranite (Fig. 16). The second group did not achieve isotope homogeneity and the amount of mafic material involved is significant. Both groups appear to have been batches of magma that chilled at slightly different stages of mixing within the same intrusive unit.

8. Origin of primary felsic magmas

8.1. The source of granite

The $(^{87}Sr/^{86}Sr)_i$ ratios and $\epsilon_{Nd}(t)$ and $\delta^{18}O$-values that are very similar for U_1 and U_2 granitoid-rock compositions (Figs. 8 and 10), indicate a single source, but raise the question of how

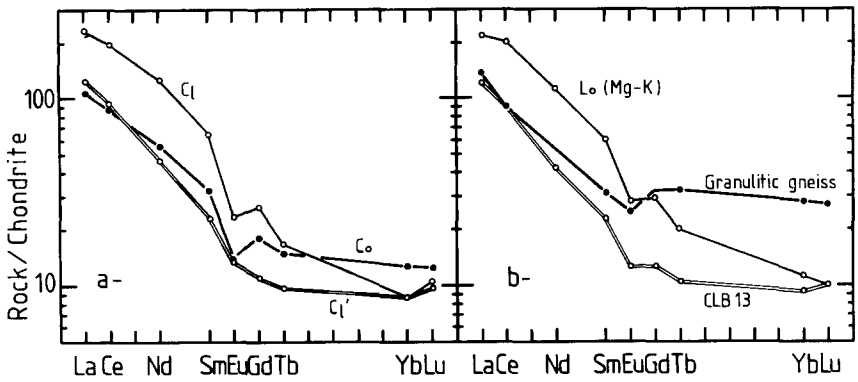

Fig. 18. a. Calculated REE patterns for granitoid rock according to a non-modal batch partial-melting model with $F=0.3$. The initial-solid source has a graywacke composition (Table 9). Two different liquids are obtained as a function of metamorphic conditions: (1) a high Mg–K liquid (C_l) in the granulite facies; and (2) a calc-alkaline liquid (C_l') under high p_{H_2O} conditions. b. Calculated REE patterns are compared to the initial liquid L_0 and the analysed rock sample CLB *13* (Table 9). Some Corsican granulitic paragneiss (Table 2) could be regarded as representative of a possible protolith.

to obtain such different magmas from the same solid source. The present idea is that, during partial melting, the trace-element content of the resulting magma will strongly depend on the percentage of some residual phase (feldspar for Sr, Eu; biotite for Rb, Ba; amphibole and garnet for REE). Two very similar solid sources, or a single one, could successively undergo two metamorphic events, one at high pressure and low p_{H_2O}, and the second under more hydrous conditions. Winkler (1967), as well as Arth and Hanson (1975) showed that granite melts can be produced by partial melting of graywacke-type rock. Precambrian (Wildeman and Haskin, 1973; Arth and Hanson, 1975) and Archaean (Wildeman and Condie, 1973) graywackes were analysed for REE.

The ΣREE of such rocks can vary from 44 to 400 ppm with LREE fractionated patterns, HREE being less fractionated for the most enriched patterns, and with a negative Eu anomaly that decreases with decreasing total REE contents. The average REE pattern of quartz-rich and quartz-intermediate graywackes is taken as representative of the average REE-distribution pattern of our solid source (S.R. Taylor and McLennan, 1985). Fig. 18a shows two models for the melting of rock with a graywacke composition, (C_l) being a dry initial assemblage (granulite) and (C_l') a hydrous assemblage (amphibolite facies). The best fit is obtained for 30% partial melting in both cases (granulite and amphibolite facies): Fig. 18a and b showing the calculated and experimental REE data, respectively. Similar calculations were done for Rb, Sr and Ba (Table 9), and the two sets of values perfectly agree. However, there is a discrepancy between calculated Sr and Eu values for the amphibolite-facies model, and their concentrations in analysed samples. Two explanations are possible: either much more plagioclase is present in the initial source, or the partition coefficients $K_d^{Plag/Liq}$ for Sr and Eu (1.42 and 0.69, respec.) are underestimated. With higher K_d-values of 5.4 and 1.9, which are realistic for granitic melts according to Arth (1976), calculated data would agree with experimental concentrations.

A possible source, i.e. a high T–low P granulitic paragneiss (Libourel, 1985), was analysed for trace elements (Table 1); the Rb, Sr, Ba and REE analyses were compared with the modelled graywacke source (Table 9). The REE patterns of Corsican granulite define a field close to the REE pattern of graywacke, except for their higher HREE content (Fig. 18). When melting in granulite facies, such paragneiss could give a monzodioritic liquid, and melting in amphibolite facies would lead to a monzogranitic liquid. As previously suggested (Cocherie and Rossi, 1991), the composition of U_1 and U_2 granites appears to be

Table 9
Trace-element calculations using a non-modal batch partial melting model to produce the initial granitic liquids of U_1 and U_2 compositions

	K_d			Gneiss	C_0	Granulitic model				Amphibolite facies model			
	ortho-pyroxene	garnet	apatite			D_0	P	C_l (F=0.3)	L_0	D'_0	P'	C'_l (F=0.3)	L_0 CLB *13*
Rb	0.0027	0.0085	-	41	63	0.058	0.136	198	170	0.752	0.485	69	91
Sr	0.0085	0.015	-	245	222	0.963	1.852	313	550	0.533	0.383	309	190
Ba	0.0029	0.017	-	451	588	0.861	2.268	1223	1500	0.661	0.436	708	647
La	0.10	(0.30)	(30.0)	43.4	34	0.209	0.168	74.1	70	0.651	0.259	38.9	38.4
Ce	0.15	0.35	34.7	70.7	68	0.177	0.120	154	160	0.717	0.276	72.8	69.3
Nd	0.22	0.53	57.1	-	32	0.160	0.061	72.5	65	1.012	0.332	26.4	24.4
Sm	0.27	2.66	62.8	5.73	5.8	0.222	0.055	11.5	11	1.223	0.434	4.16	4.18
Eu	0.17	1.50	30.4	1.80	0.95	0.471	0.637	1.63	2	0.837	0.386	0.93	0.87
Gd	0.34	10.5	56.3	-	4.55	0.415	0.046	6.50	7.5	1.545	0.672	2.77	3.18
Tb	(0.40)	(18.0)	52.0	1.63	0.74	0.603	0.042	0.83	1	1.406	0.541	0.48	0.51
Yb	0.86	39.9	23.9	5.49	2.45	1.176	0.025	1.67	2.2	1.277	0.490	1.71	1.83
Lu	0.90	29.6	20.2	0.91	0.41	0.924	0.027	0.34	0.33	1.164	0.520	0.32	0.33

K_d=partition coefficients, taken from Arth (1976); those for plagioclase, K-feldspar, biotite and amphibole are listed in Table 4; interpolated values are in brackets. Gneiss: corresponds to the average value of Corsican granulitic paragneiss (Table 2). C_0=trace-element concentrations of the initial solid source material (average concentrations of quartz-rich and quartz–intermediate graywackes; S.R. Taylor and McLennan, 1985). Corsican granulitic gneisses are compared with the selected trace-element concentrations (see text for explanation). D_0=bulk distribution coefficients for the dry initial assemblage (Qz, 35%; Pl, 35%; K-fs, 12%; Opx, 15.4; Gt, 2.5%; Ap, 0.1%). P=bulk distribution coefficients corresponding to the following proportions of minerals contributing to the melt: Qz, 30%; Pl, 35%; K-fs, 35%. C_l=calculated trace-element contents of the melt according to the dry model compared with the L_0 content of the primitive monzodiorite melt (Table 3).
D'_0, P'=bulk distribution coefficients calculated with the following mineral assemblage; Qz, 35%; Pl, 36%; Bio, 14%; Amph, 13%; Gt, 1%; Ap, 1% and Qz, 55%; Pl, 26%; Bio, 9%; Amph, 10%. C'_l=calculated trace-element contents of the melt according to the hydrous model compared with the L_0 CLB *13* contents of the primitive monzogranite melt.

more likely controlled by physico-chemical fusion parameters than by composition of the protolith.

8.2. Age of the granite source material

The possible source involved in granitoid-magma genesis has a graywacke composition (Rb=63 ppm; Sr=222 ppm). This leads to a $^{87}Rb/^{86}Sr$ ratio of 0.82, which can be compared to that obtained from average Rb and Sr contents of Corsican granulitic gneiss (Rb=41 ppm; Sr=245 ppm; $^{87}Rb/^{86}Sr$ ratio of 0.48). About 322 Ma ago (i.e. the U_1 age) the initial $^{87}Sr/^{86}Sr$ ratio was close to 0.707. If we consider a two-stage model, the protolith being derived from a depleted-type mantle with a Sr_i of 0.7028, the average age of the source material is calculated to be $\sim 800 \pm 100$ Ma, based on a Rb/Sr ratio of 0.48 or 0.82. This is a minimum age, because acid–basic magma interaction may have lowered the initial Sr ratio of the granite. Inherited zircons from continental crust found in U_2 gabbro of the Peloso CMU gave an age of 1000 Ma (Rossi et al., 1992), which agrees with such calculations. This strontium model age can be compared with the Nd model age (Fig. 19). For each analysed sample, the evolution line is drawn from t=0–300 Ma in the $\epsilon_{Nd}=f(t)$ diagram. As listed in Table 3, the average $\epsilon_{Nd}(t)$ is close to -3.5, t being the assumed granite age. Using the average Sm/Nd ratio of the granulitic paragneiss, taken as representative of the source protolith, we can calculate the $^{147}Sm/^{144}Nd$ ratio (0.115), which provides a model for the time evolution of the protolith; its intercept with the depleted mantle (D.M.) growth curve gives a model age of ~ 1100 Ma. This age is close to the calculated t_{DM} ages (Table 3) of each individual sample, as the Sm/Nd ratios of the rocks in question are similar to those of assumed source rocks. There is no significant difference between Nd and Sr model ages, because the evolution band for depleted mantle in the $\epsilon_{Nd}=f(t)$ diagram is very wide. The estimated age of the protolith can thus be considered as close to 1000 Ma. Note that, as discussed

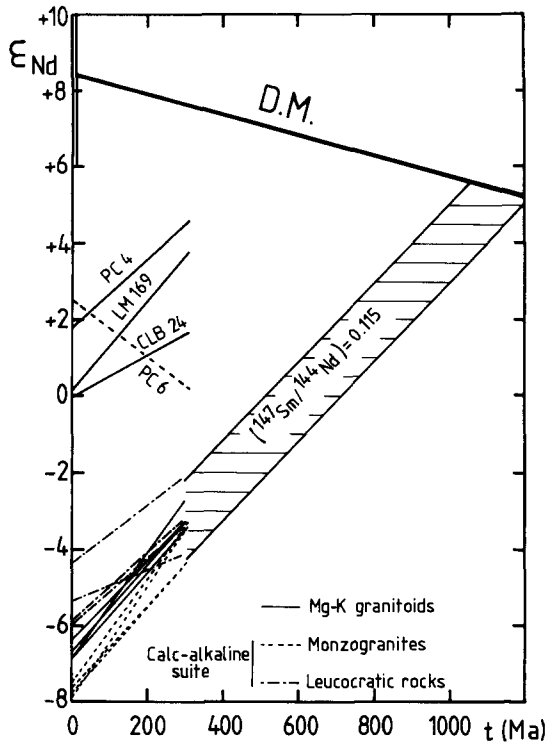

Fig. 19. ϵ_{Nd} vs. t diagram for 4 basic rocks and 12 granitoid rocks. Using $^{147}Sm/^{144}Nd=0.115$ as previously defined for the source material (Table 9; Fig. 18), we obtain a model age around 1100 Ma near the t_{DM} (Table 3), calculated for each individual sample insofar as the Sm/Nd ratios are similar in analysed samples and the protolith. The basic rock associated with the U_2 association takes root not far from the mantle evolution trend (PC *4*, LM *169*, CLB *24*). Note that olivine-rich rock of peridotite composition (PC *6*) shows a negative slope. This evolution is rare and linked to the high $^{147}Sm/^{144}Nd$ ratio (0.2549), much higher than that of the CHUR ratio (0.1967). Its chondrite-normalized REE pattern is plotted in Fig. 6a.

by Arndt and Goldstein (1987), not all Nd model ages are necessarily "crust-formation ages", because they represent a mixture of material derived from the mantle at various times, corresponding to major orogenic events.

8.3. Comparison between Corsican, Sardinian and Pyrenean Hercynian batholiths

Before the Oligocene–Miocene oceanization in the western Mediterranean region, continuous Variscan crust existed between Corsica, Sardinia and the Pyrénées, opening the possibility to investigate a large section of the Variscan orogenic belt.

Geochemical data on Pyrenean Variscan plutons were summarized in Cocherie et al. (1984) and Cocherie and Autran (1994). It can be seen that the calc-alkaline geochemical trends of Pyrenean plutons are similar to those of the Budduso massif in northeastern Sardinia (Cocherie, 1984; Poli et al., 1989) and those of the Corsican U_2 unit discussed here. The otherwise uniform geochemical behaviour of the Hercynian plutons in Corsica, Sardinia and the Pyrénées, is not confirmed by Sr, Nd and O isotope data. For Sardinia, the Sr initial ratio of 0.7096 from the Budduso massif (Cocherie, 1984) is close to the unpublished values cited by Brotzu et al. (1983) from the Sarrabus massif (0.7092–0.7098), and those for the Bono intrusive complex (0.7073–0.7090; Bouchet et al., 1992). These Sr initial ratios fall between those from Corsica (0.707) and the Pyrénées (0.711) (Fig. 8). The $\delta^{18}O$-values show similar geochemical trends in rock of granodioritic to monzogranitic composition: average $\delta^{18}O$-values scatter from +7.7‰ for Corsican granite to +9.3‰ for Pyrenean granite, with an intermediate value of +8.9‰ for Sardinia (Brotzu et al., 1983). A similar evolution from Corsica to the Pyrénées is seen when considering Sm–Nd isotope data. $\epsilon_{Nd}(t)$ increases from average values of −5.6 for the Pyrenean Quérigut pluton (Ben Othman et al., 1984), −6.2 for the Trois Seigneurs Massif (Bickle et al., 1988) and −5.6 for granodiorite from the Bono complex in Sardinia (Bouchet et al., 1992), to −3.5 in the Corsican batholith.

U_2-type granite remains very similar throughout the Variscan chain from Corsica–Sardinia to the Pyrénées, from a petrological, mineralogical and major- and trace-element geochemistry point of view. Broad-scale zoning, revealed by isotopes, was inherited from deep sources of the granite. Such regional isotope zonation indicates that batholiths were generated along boundaries of the eastern "Austro-Alpine" and western "Ebro-Aquitanian" terranes (Rossi and Cocherie, 1991); granite of the Corsican batholith

would belong to the first terrane, and granites in Sardinia and the Pyrénées to the second one.

9. Conclusions

Our work on the Corsican batholith and other plutons of the southern realm of the Variscan chain, has led to insight into Variscan continental growth through the origin and emplacement of so-called "calc-alkaline" plutonic associations.

Successively emplaced U_1 and U_2 magmatic associations are the result of mixing of non-cogenetic mafic and silicic magmas. Two different types of mantle were melted to give mafic end-members: U_1 "lamprophyric" ultra-K magma resulted from fusion of a phlogopite (±garnet) metasomatized mantle and, in a second stage, a zone-refining process led to significant increase of incompatible trace-element contents. Finally, the magma interacted with the base of the crust, leading to lower La/Yb and $^{147}Sm/^{144}Nd$, and higher $^{87}Sr/^{86}Sr$ ratios in the melt. U_2 "E-MORB" magma resulted from non-modal partial melting of a spinel or amphibolite lherzolitic mantle. Primitive silicic magmas of both U_1 and U_2 have similar relatively low $^{87}Sr/^{86}Sr$ ratio (0.706–0.707), as well as low $\delta^{18}O$ (+7 to +8‰) and high $\epsilon_{Nd}(t)$ (−4.3 to −2.2) values. They derived from the same continental source that melted under different conditions of fusion, leading to different initial liquids, i.e. monzodioritic for U_1 and monzogranitic for U_2. This emphasizes the importance of fluid content and *P–T* melting conditions, when anatexis of continental crust is involved in the generation of granitic melts.

Intermediate rocks (granodiorite) in both U_1 and U_2 resulted from mixing of pre-existing rocks of mafic and silicic composition. Isotope and major- and trace-element geochemistry support evidence of mixing processes in U_2, but in U_1 the mafic and silicic end-members were completely blended. Microgranular enclaves of intermediate to acid rocks of each association, in the shape of undisrupted bubbles of mafic magma chemically equilibrated in a silicic environment, remained as "fossilized" remnants of such processes. Such magma of intermediate composition bridges the gap between mafic and silicic end-members. In such a case, the "calc-alkaline trend" that was obtained is quite different from the calc-alkaline trend of American coastal batholiths, which are related to subduction beneath a continental margin and result from fractional crystallization of a basalt source. This example from Variscan plutonism shows that unconsidered use of the term "calc-alkaline" can be misleading.

Isotopic constraints give an estimated age for the protolith of ~1 Ga, and indicate that the Corsican protolith is younger than the Sardinian and Pyrenean batholiths, providing evidence for crustal-accretion processes.

The major difference between the two assumed mantle sources that yielded mafic U_1 and U_2 magmas agrees with progressive uplift of the asthenosphere, i.e. in a lithosphere under extensional stress. This lead to melting of a deep phlogopite (garnet) U_1 mantle around 322 Ma, then to melting of the shallower garnet-free spinel lherzolitic U_2 mantle (312–280 Ma), and finally to the U_3 alkaline volcanic–plutonic episode (280–250 Ma). This constrained the emplacement of the last part of U_2 calc-alkalic plutonism to post-collisional crustal-thinning conditions.

Acknowledgements

We thank A. Autran for helpful discussions and suggestions. F. Vidal is acknowledged for Nd analyses. We are also grateful to the "Groupe des Sciences de la Terre" of the P. Süe laboratory (Saclay, France) and to the CAESS of Rennes (France), where respectively trace elements and Sr isotopes were analysed by A.C. A.C. and Ph.R. thank the C.N.R.S., Centre de Recherches sur la Synthèse et la Chimie des Minéraux, laboratories at Orléans, where part of the study was carried out. We thank very much the two anonymous reviewers who help us to improve the first version of the manuscript. This is B.R.G.M. contribution No. 931015; the work was financially supported by a B.R.G.M. research grant.

Appendix A — Petrographical and mineralogical data on U_1 and U_2 rocks

Analytical data not presented in Tables 1 and 2 are available in Cocherie et al. (1984) and Rossi and Cocherie (1991). Precise sample locations are given in Rossi (1986). Modal compositions for samples are indicated by an asterisk (*).

U_1 *association*

Intermediate to acid rocks have a typical mineralogical distribution: abundant apatite and zircon as earliest minerals; augite clinopyroxene surrounded by actinolitic hornblende (up to monzogranite composition); Ca-plagioclase (An_{30}-monzonite to An_{10}-syenogranite); Ba-rich K-feldspar; foxy-red Mg–Ti-biotite ($X_{Fe} \approx 0.50$); ilmenite is the most abundant oxide; sulphides and macroscopic titanite are ubiquitous.

Ultrapotassic rocks (melasyenite to melamonzonite) display some common characteristics throughout the different massifs: "primary minerals" are Cr-diopside to augite clinopyroxene, Ca-plagioclase, Ba-rich K-feldspar, foxy-red Mg–Ti-biotite, and rare relics of phlogopitic mica. Ilmenite, commonly surrounded by sphene, is the most abundant oxide; magnetite is scarce. Of particular interest is the occurrence of Cr-spinel in micaceous aggregates, which could represent relics of olivine. Sulphides are ubiquitous. Apatite and zircon are the earliest minerals. The systematic presence of actinolitic hornblende is characteristic of such rocks. Typically secondary biotites are different in habit, such as those that occur in mineral cracks or aggregates. The earliest minerals are: zircon, thorite, allanite, apatite, sphene and sulphides (pyrrhotite + chalcopyrite + exsolutions of pentlandite) and oxides (ilmenite and rutile with exsolutions of ilmenite).

(K *1*, K *5*, K *6*, K *4*, K *25**): plagioclase 13%, K-feldspar 29%, quartz 4%, biotite 28%, magnesian hornblende–amphibole with relict Cr-diopside 23%, apatite 1%, ilmenite and titanite 2%.

U_2 *association*

Intermediate to acid rocks: in granodiorite, plagioclase is An_{20-60}-amphibole and biotite (both with $X_{Fe} = 0.5–0.7$) nearly everywhere occur together as aggregates; magnetite, allanite, apatite and titanite are accessories. Amphibole is rare in monzogranite. The composition of biotite-bearing leucomonzogranite is close to thermal minimum in the Qz–Ab–Or–H_2O system; almandine–spessartine garnet can occur as an accessory phase.

Ultramafic and mafic rocks: peridotite (PC *6**) has a heteradcumulate texture, cumulate olivine 60% (Fo_{83}); intercumulus clinopyroxene partly replaced by pargasitic hornblende, plagioclase (An_{58-70}), Cr-spinel, ilmenite, magnetite and sulphides.

Troctolite (PC *4*, PC *7*, LM *169**): mesocumulate texture, plagioclase 70% (An_{75-78}), olivine 23% (Fo_{80}), orthopyroxene, clinopyroxene.

Gabbro (assumed liquid composition, PC *5*, CLB *24**): texture of orthocumulate, plagioclase 42% (An_{40-65}), olivine 7% (Fo_{68}), clinopyroxene 15%, orthopyroxene 6%, brown amphibole 29%, ilmenite, magnetite, green spinel and sulphides.

Gabbronorite (P *6*): orthocumulate texture, plagioclase (An_{52-57}), olivine (Fo_{56}), orthopyroxene, clinopyroxene, poikilitic brown hornblende, apatite, ilmenite, biotite.

Gabbronorite (P *1*): cumulate texture showing strong igneous lamination, plagioclase (An_{50-52}), orthopyroxene (proportions equivalent to plagioclase), clinopyroxene, poikilitic brown hornblende and biotite, apatite, quartz.

Orthopyroxene-bearing granodiorite (CLB *27*): medium- to coarse-grained texture, plagioclase 48% (An_{30-40}), K-feldspar 15%, quartz 21%, orthopyroxene 7%, clinopyroxene 1% etched by green amphibole 7%, biotite and opaques 1%.

Norite (PV *532*, CLB *18*, CLB *20**): heteradcumulate texture, cumulate olivine 7% (Fo_{71}), cumulative plagioclase 40% (An_{90-95}), poikilitic orthopyroxene 15%, heteradcumulate pargasitic hornblende 31% partly replacing relict clinopyroxene 4%, ilmenite, magnetite, sulphides, green spinel.

Gabbro (CLB *5*, CLB *7**): coarse-grained texture, plagioclase 44% (relict core An_{82}, large rim An_{49-51}), magnesian hornblende 40% including relict orthopyroxene, biotite 6%, ilmenite, magnetite.

Gabbro-diorite and diorite (CLB *40*, CLB *43**, CLB *15*): fine- to medium-grained texture, plagioclase 48% (An_{46-53}, some relict cores An_{80}), ferrohornblende, amphibole 28%, biotite 21%, quartz 2%, ilmenite and magnetite 1%.

Diorite (CLB *30**, CLB *34*): fine- to medium-grained texture, plagioclase 52% (An_{37-43}, some relict cores An_{69}), green amphibole 15%, poikilitic biotite 13%, poikilitic K-feldspar 3%, quartz, apatite, titanite, ilmenite, magnetite.

Appendix B — Inverse geochemical approach

The direct geochemical approach using trace elements requires a choice of: magmatic model, realistic F-values (weight fraction of the residual liquid F), appropriate bulk-distribution coefficients D (using published individual mineral/melt partition coefficients), and verification that the analysed rocks fit the predicted model and parameters. We consider that it is more suitable, when possible, to use an inverse approach (Treuil and Varet, 1973; Treuil et al., 1979), examining the data distribution in appropriate diagrams, in order to identify the main evolutionary process. Allègre et al. (1977), Cocherie (1986), etc., have shown that the main evolutionary process is easily identified by plotting trace-element couples of very different D-value. Furthermore, in the case of fractional crystallization, the parameters of the main evolutionary process (D, F, C_i, C_f) can be determined graphically (Cocherie, 1986), without having to make any assumptions concerning the initial magma and the proportions of the minerals in equilibrium with the evolving melt. In this manner, it becomes possible to discuss the possible source material of primary liquids.

References

Alibert, C., Michard, A. and Albarède, F., 1983. The transition from alkali basalts to kimberlites: isotope and trace element evidence from melilites. Contrib. Mineral. Petrol., 82: 176–186.

Allègre, C.J. and Ben Othman, D., 1980. Nd–Sr isotopic relationship in granitoid rocks and continental crust development: a chemical approach to orogenesis. Nature (London), 287: 335–342.

Allègre, C.J., Treuil, M., Minster, J.F., Minster, J.B. and Albarède, F., 1977. Systematic use of trace element in igneous process, Part I: Fractional crystallization processes in volcanic suites. Contrib. Mineral. Petrol., 60: 57–75.

Arndt, N.T. and Goldstein, S.L., 1987. Use and abuse of crust-formation ages. Geology, 15: 893–895.

Arth, J.G., 1976. Behavior of trace elements during magmatic processes — a summary of theoretical models and their applications. J. Res. U.S. Geol. Surv., 4(1): 41–47.

Arth, J.G. and Hanson, G.N., 1975. Geochemistry and origin of early Precambrian crust of northeastern Minnesota. Geochim. Cosmochim. Acta, 39: 325–362.

Autran, A., Fonteilles, M. and Guitard, G., 1970. Relations entre les intrusions de granitoïdes, l'anatexie et le métamorphisme régional, considérés principalement du point de vue du rôle de l'eau: cas de la chaîne des Pyrénées orientales. Bull. Soc. Géol. Fr., 12: 673–671.

Banzet, G., 1987. Interactions croûte–manteau et genèse du plutonisme subalcalin du Haut-Dauphiné occidental (massifs cristallins externes, Alpes): vaugnérites, durbachites et granitoïdes magnésio-potassiques. Géol. Alp., 63: 95–117.

Ben Othman, D., Fourcade, S. and Allègre, C.J., 1984. Recycling processes in granite–granodiorite complex genesis: the Querigut case studied by Nd–Sr isotope systematics. Earth Planet. Sci. Lett., 69: 290–300.

Bergman, S.C., 1987. Lamproites and other potassium-rich igneous rocks: a review of their occurrence, mineralogy and geochemistry. In: J.G. Fitton and B.G.J. Upton (Editors), Alkaline Igneous Rocks. Geol. Soc. London, Spec. Publ., 30: 103–190.

Bernard-Griffiths, J., 1975. Essai sur la signification des âges au strontium dans une série métamorphique: le bas Limousin (Massif Central français). Doctoral Thesis, University of Clermont-Ferrand, Clermont-Ferrand, 243 pp.

Bickle, M.J., Wickham, S.M., Chapman, H.J. and Taylor, Jr., H.P., 1988. A strontium, neodymium and oxygen isotope study of hydrothermal metamorphism and crustal anatexis in Trois Seigneurs massif, Pyrenees, France. Contrib. Mineral. Petrol., 100: 399–417.

Bouchet, G., Duthou, J.L. and Orsini, J.B., 1992. Apport de la géochimie isotopique (Sr, Nd) à la genèse du pluton calco-alcalin carbonifère de Bono (Sardaigne septentrionale). Réun. Sci. Terre, Toulouse, Soc. Géol. Fr., Paris, 26 pp.

Bouska, V., Jelinek, E., Pacesova, M., Randa, Z. and Ulrych, J., 1984. Rare earth elements and other trace elements in the rocks of the central Bohemian pluton. Geol. Carpathica, 35: 355–376.

Brotzu, P., Ferrini, V. and Masi, U., 1983. Stable isotope geochemistry of Hercynian granitoid rocks from the Sarrabus Massif (southeastern Sardinia, Italy). Isot. Geosci., 1: 77–90.

Chayla, B., Jaffrezic, H. and Joron, J.L., 1973. Analyse par activation dans les neutrons épithermiques — Application à la détermination d'éléments en traces dans les roches. C.R. Acad. Sci., Paris, 277: 273–275.

Clayton, R.N. and Mayeda, T.K., 1963. The use of bromine pentafluoride in the extraction of oxygen from oxides and silicates for isotopic analysis. Geochim. Comochim. Acta, 27: 45–53.

Cocherie, A., 1978. Géochimie des terres rares dans les granitoïdes. Ph.D. Thesis, University of Rennes I, Rennes, 207 pp.

Cocherie, A., 1984. Interaction manteau–croûte: son rôle dans la genèse d'associations plutoniques calco-alcalines, contraintes géochimiques (éléments en traces et isotopes du strontium et de l'oxygène). Doctoral Thesis, University of Rennes I, Rennes, 246 pp. [Doc. BRGM (Bur. Rech. Géol. Min.) No. 90 (1985)].

Cocherie, A., 1986. Systematic use of trace element distribution patterns in log–log diagrams for plutonic suites. Geochim. Cosmochim. Acta, 50: 2517–2522.

Cocherie, A. and Autran, A., 1994. Géochimie des éléments en traces. In: F. Debon (Coordinator), Synthèse géologique et géophysique des Pyrénées, Ch. 9. BRGM (Bur. Rech. Géol. Min.)–ITGE (Inst. Tec. Geomin. España), Orléans (in press).

Cocherie, A. and Rossi, Ph., 1991. Origin of Variscan ultrapotassic and high-potassic plutonic association related to post-collisional environment: trace element and isotope evidence. Terra Abstr., 3: 17.

Cocherie, A., Rossi, Ph. and Le Bel, L., 1984. The Variscan calc-alkalic plutonism of Western Corsica: Mineralogy and major and trace element geochemistry. Phys. Earth Planet. Inter., 35: 145–178.

Cocherie, A., Guerrot, C. and Rossi, Ph., 1992. Single zircon dating by step-wise Pb evaporation: comparison with other geochronological techniques applied to the Hercynian granites of Corsica. In: R.S. Harmon and R.W. Hinton (Guest-Editors), Frontiers in Isotope Geosciences. Chem. Geol. (Isot. Geosci. Sect.), 101: 131–141 (special issue).

Cocherie, A., Wickham, S.M. and Autran, A., 1994. Géochimie des isotopes stables et radiogéniques. In: F. Debon (Coordinator), Synthèse géologique et géophysique des Pyrénées, Ch. 9. BRGM (Bur. Rech. Géol. Min.)–ITGE (Inst. Tec. Geomin. España), Orléans (in press).

Cole, J.W., Cashman, K.V. and Rankin, P.C., 1983. Rare-earth element geochemistry and the origin of andesites and basalts of the Taupo volcanic zone, New Zealand. Chem. Geol., 38: 255–274.

Crawford, A.J., Falloon, T.J. and Eggins, S., 1987. The origin of island arc high-alumina basalts. Contrib. Mineral. Petrol., 97: 417–430.

Cullers, R.L. and Graf, J.L., 1984. Rare earth elements in igneous rocks of the continental crust: predominately basic and ultrabasic rocks. In: P. Henderson (Editor), Rare Earth Element Geochemistry, Ch. 7. Elsevier, Amsterdam, pp. 237–274.

Debon F., 1975. Les massifs granitoïdes à structure concentrique de Cauterets–Panticosa (Pyrénées occidentales) et leurs enclaves. Sci. Terre, Nancy, Mém., 33, 420 pp.

Deniel, C., Vidal, P., Fernandez, A., Le Fort, P. and Peucat, J.J., 1987. Isotopic study of the Manaslu granite (Himalaya, Nepal): inferences on the age and source of Himalayan leucogranites. Contrib. Mineral. Petrol., 96: 78–92.

DePaolo, D.J., 1981a. Nd in the Colorado Front Range and implications for crust formation and mantle evolution in the Proterozoic. Nature (London), 294: 193–196.

DePaolo, D.J., 1981b. A Nd and Sr isotopic study of the Mesozoic calc-alkaline granitic batholiths of the Sierra Nevada and Peninsular Ranges, California. J. Geophys. Res., 86: 10470–10488.

Foley, S.F., Venturelli, G., Green, D.H. and Toscani, L., 1987. The ultrapotassic rocks: characteristics classification, and constraints for petrogenetic models. Earth-Sci. Rev., 24: 81–134.

Fourcade, S., 1981. Géochimie des granitoïdes. Doctoral Thesis, University of Paris VII, Paris, 189 pp.

Fourcade, S. and Allègre, C.J., 1981. Trace element behavior in granite genesis — a case study: the calc-alkalic plutonism association from the Querigut complex (Pyrenées, France). Contrib. Mineral. Petrol., 76: 177–195.

Govindaraju, J., Mevelle, G. and Chouard, C., 1976. Automated optical emission spectrochemical bulk analyses of silicate rocks with microwave plasma excitation. Anal. Chem., 48: 1325–1331.

Green, T.H., 1980. Island arc and continent-building magmatism — a review of petrogenetic models based on experimental petrology and geochemistry. Tectonophysics, 63: 367–385.

Gromet, L.P. and Silver, L.T., 1983. Rare earth element distribution among minerals in a granodiorite and their petrogenetic implications. Geochim. Cosmochim. Acta, 47: 925–939.

Gromet, L.P., Dymek, R.F., Haskin, L.A. and Korotev, R.L., 1984. The "North American shale composite": its compilation, major and trace element characteristics. Geochim. Cosmochim. Acta, 48: 2469–2482.

Harker, A., 1909. The Natural History of the Igneous Rocks. Methuen, London, 384 pp.

Harris, P.G., 1974. Origin of alkaline magmas as a result of anatexis (mantle anatexis). In: H. Sorenson (Editor), The Alkaline Rocks. Wiley, New York, N.Y., pp. 427–436.

Hawkesworth, C.J. and Vollmer, R., 1979. Crustal contamination versus enriched mantle: $^{143}Nd/^{144}Nd$ and $^{87}Sr/^{86}Sr$ evidence from the Italian volcanics. Contrib. Mineral. Petrol., 69: 151–165.

Jacobsen, S.B. and Wasserburg, G.J., 1984. Sm–Nd isotopic evolution of chondrites and achondrites, II. Earth Planet. Sci. Lett., 67: 137–150.

Jaffrezic, H., Joron, J.L., Treuil, M. and Wood, D.A., 1980. A study of the precision attained by neutron activation analysis using international standard rocks GSN and BCR-*1* as examples. J. Radioanal. Chem., 55: 417–425.

Jahn, B.M., Sun, S.S. and Nesbitt, R.W., 1979. REE distribution and petrogenesis of the Spanish Peaks igneous complex, Colorado. Contrib. Mineral. Petrol., 70: 281–298.

Jahn, B.M., Bernard-Griffiths, J., Charlot, R., Cornichet, J. and Vidal, F., 1980. Nd and Sr isotopic compositions and REE abundances of Cretaceous MORB (Holes *417*D and *418*A, Legs *51*, *52* and *53*). Earth Planet. Sci. Lett., 48: 171–184.

Jakes, P. and Gill, J., 1970. Rare earth elements and the island arc tholeiitic series. Earth Planet. Sci. Lett., 9: 17–28.

Joron, J.L. and Treuil, M., 1977. Utilisation des propriétés des éléments fortement hygromagmatophiles pour l'étude de la composition chimique et l'héterogénéité du manteau. Bull. Soc. Géol. Fr., 19: 1197–1205.

Kay, W.R. and Gast, P.W., 1973. The rare earth content and origin of alkali-rich basalts. J. Geol., 81: 653–682.

Laporte, D., 1987. Un exemple d'intrusion syntectonique: l'intrusion d'Île-Rousse, Corse du Nord-Ouest — Étude pétrographique, minéralogique et géochimique — Analyse structurale. Doctoral Thesis, University of St. Étienne, St. Étienne, 422 pp.

Le Bel, L., Cocherie, A., Baubron, J.C., Fouillac, A.M. and Hawkesworth, C.J., 1985. A high-K, mantle derived plutonic suite from "Linga", near Arequipa, Peru. J. Petrol., 26: 124–148.

Leterrier, J., 1972. Étude pétrographique et géochimique du massif granitique du Querigut. Sci. Terre, Nancy, Mém. 23, 300 pp.

Libourel, G., 1985. Le complexe de Santa Lucia di Mercurio (Corse) — Ultramafites mantelliques, intrusion basique stratifié, paragneiss granulitiques — Un équivalent possible des complexes de la zone d'Ivrée. Ph.D. Thesis, University of Toulouse, Toulouse, 405 pp.

Marre, J., 1973. Le complexe éruptif du Querigut — Pétrologie, structurologie, cinématique de mise en place. Doctoral Thesis, University of Toulouse, Toulouse, 536 pp.

Marre, J. and Rossi, Ph., 1981. Extension et anteriorité relative du plutonisme subalcalin potassique dans l'ensemble des granitoïdes de Corse. C.R. Acad. Sci., Paris, Sér. II, 291: 1015–1018.

Marre, J., Bourges, F. and Rossi, Ph., 1981. Architecture et chronologie des intrusions des granitoïdes varisques en Corse sud-occidentale — Processus de formation d'un secteur de batholite. Rend. Soc. Ital. Mineral. Petrol., 38: 119–132.

McKenzie, D., 1989. Some remarks on the movement of small melt fractions in the mantle. Earth Planet. Sci. Lett., 95: 53–72.

Michard-Vitrac, A., Albarède, F., Dupuis, Ch. and Taylor, H.P., Jr., 1980. The genesis of Variscan (Hercynian) plutonic rocks: Inferences from Sr, Pb and O studies on the

Maladeta igneous complex, Pyrenees (Spain). Contrib. Mineral. Petrol., 72: 57–72.

Miller, C.F. and Mittlefehldt, D.W., 1982. Light rare earth element depletion in felsic magmas. Geology, 10: 129–133.

Mitchell, R.H. and Bell, K., 1976. Rare earth element geochemistry of potassic lavas from the Birunga and Toro–Ankole regions of Uganda, Africa. Contrib. Mineral. Petrol., 48: 293–303.

Mitchell, R.H., Platt, R.G. and Downey, M., 1987. Petrology of lamproites from Smoky Butte, Montana. J. Petrol., 28: 645–677.

Mittlefehldt, D.W. and Miller, C.F., 1983. Geochemistry of the Sweetwater Wash pluton, California: implications for "anomalous" trace element behavior during differentiation of felsic magmas. Geochim. Cosmochim. Acta, 47: 109–124.

Neal, C.R. and Davidson, J.P., 1989. An unmetasomatized source for the Malaitan alnöite (Solomon Islands): petrogenesis involving zone refining, megacryst fractionation, and assimilation of ocean lithosphere. Geochim. Cosmochim. Acta, 53: 1975–1990.

Newsom, H.E., White, W.M., Jochum, K.P. and Hofmann, A.W., 1986. Siderophile and chalcophile element abundances in ocean basalts, Pb isotope evolution and growth of the Earth's core. Earth Planet. Sci. Lett., 80: 299–313.

Nicholls, I.A., Whitford, D.J., Harris, K.L. and Taylor, S.R., 1980. Variation in the geochemistry of mantle sources for tholeiitic and calc-alkaline mafic magmas, western Sunda arc, Indonesia. In: R.W. Le Maitre and A. Cundari (Guest-Editors), Chemical Characterization of Tectonic Provinces. Chem. Geol., 30: 177–199 (special issue).

O'Hara, M.J. and Yoder, H.S., 1967. Formation and fractionation of basic magmas at high pressures. Scott. J. Geol., 3: 67–117.

Orsini, J.B., 1980. Le batholite corso–sarde: un exemple de batholite hercynien (structure, composition, organisation d'ensemble) — Sa place dans la chaîne varisque de l'Europe moyenne. Doctoral Thesis, University of Aix-Marseille III, Marseille, 370 pp.

Pagel, M., 1982. The mineralogy and geochemistry of uranium, thorium and rare earth elements in two radioactive granites of Vosges, France. Mineral. Mag., 46: 149–161.

Pagel, M. and Leterrier, J., 1980. The subalkaline potassic magmatism of the Ballons massif (southern Vosges, France): shoshonitic affinity. Lithos, 13: 1–10.

Philpotts, J.A., Martin, W. and Schnetzler, C.C., 1971. Geochemical aspects of some Japanese lavas. Earth Planet. Sci. Lett., 12: 89–96.

Pitcher, S.W., 1979. A commentary on the nature, ascent and emplacement of granitic magmas. J. Geol. Soc. London, 136: 627–662.

Poitrasson, F., Pin, Ch. and Duthou, J.L., 1992. Datation d'un représentant du magmatisme tholéitique du SW corse et des roches intermédiaires associées: le massif de Fozzano. 14th Réun. Sci. Terre, Toulouse, Soc. Géol. Fr., Paris, p.127.

Poli, G., Ghezzo, C. and Conticelli, S., 1989. Geochemistry of granitic rocks from the Hercynian Sardinia–Corsica batholith: implication for magma genesis. Lithos, 23: 247–266.

Rock, N.M.S., 1987. The nature and origin of lamprophyres: an overview. In: J.G. Fitton and B.J.G. Upton (Editors), Alkaline Igneous Rocks. Geol. Soc. London, Spec. Publ., 30: 191-226.

Rossi, Ph., 1986. Organisation et genèse d'un grand batholite orogénique: le batholite calco-alcalin de la Corse. Doctoral Thesis, University of Toulouse, Toulouse [Doc. BRGM (Bur. Rech. Géol. Min.), Paris, No. 107, 292 pp.].

Rossi, Ph. and Chevremont, Ph., 1987. Classification des associations magmatiques granitoïdes. Géchronique, 21: 14–18.

Rossi, Ph. and Cocherie, A., 1991. Genesis of a Variscan batholith — Field, petrological and mineralogical evidence from the Corsica–Sardinia batholith. In: R. Freeman, M. Huch and S. Mueller (Editors), The European Geotraverse. Tectonophysics, 195: 319–346.

Rossi, Ph., Cocherie, A. and Lahondère, D., 1992. Relations entre les complexes mafiques ultramafiques et le volcanisme andésitique permien de Corse occidentale, témoins des phénomènes d'amincissement crustal néo-varisques. C.R. Acad. Sci. Paris, Sér. II, 315: 1341–1348.

Rossi, Ph., Durand Delga, M. and Cocherie, A., 1993. Caractère volcano-plutonique du magmatisme calco-alcalin composite d'âge stéphanien supérieur-Permien inférieur en Corse. C.R. Acad. Sci., Paris, Sér. II, 316: 1779–1788.

Scharbert, S., 1992. Rubidium–strontium systematics of granitoid rocks of the South Bohemian plution. In: Z. Kukal (Editor), Proceedings of the 1st International Conference on the Bohemian Massif. Czech. Geol. Surv., Prague, pp. 229–231.

Shand, S.J., 1927. Eruptive Rocks. Wiley, New York, N.Y., 444 pp.

Shaw, D.M., 1970. Trace element fractionation during anatexis. Geochim. Cosmochim. Acta, 34: 237–243.

Shaw, D.M., 1980. Development of the early continental crust, Part III. Depletion of incompatible elements in the mantle. Precambrian Res., 10: 281–299.

Sheppard, S.M.F., 1986. Igneous rocks, III. Isotopic case studies of magmatism in Africa, Eurasia and oceanic islands. In: J.W. Valley, H.P. Taylor, Jr. and J.R. O'Neil (Editors), Stable Isotopes in High Temperature Geological Processes. Am. Mineral. Soc., Rev. Mineral., 16: 319–371.

Shibata, T., Thompson, G. and Frey, F.A., 1979. Tholeiitic and alkali basalts from the Mid-Atlantic ridge at 43°N. Contrib. Mineral. Petrol., 70: 127–141.

Sun, S.S. and Hanson, G.N., 1975. Origin of Ross Island basanitiods and limitations upon the heterogeneity of mantle sources for alkali basalts and nephelinites. Contrib. Mineral. Petrol., 52: 77–106.

Sun, S.S. and McDonough, W.F., 1989. Chemical and isotopic systematics of oceanic basalts: implications for mantle composition and processes. In: A.D. Sanders and M.J. Norry (Editors), Magmatism in the Ocean Basins. Blackwell, Oxford, pp. 313–345.

Taylor, Jr., H.P., 1980. The effects of assimilation of country rocks by magmas on $^{18}O/^{16}O$ and $^{87}Sr/^{86}Sr$ systematics in igneous rocks. Earth Planet. Sci. Lett., 47: 243–254

Taylor, Jr., H.P. and Sheppard, S.M.F., 1986. Igneous rocks: I. Processes of isotopic fractionation and isotope systematics. In: J.W. Valley, H.P. Taylor Jr. and J.R. O'Neil (Editors), Stable Isotopes in High Temperature Geological Processes. Am. Mineral. Soc., Rev. Mineral., 16: 227–271.

Taylor, S.R. and McLennan, S.M., 1985. The Continental Crust: Its Composition and Evolution. Blackwell, Oxford, 312 pp.

Thompson, R.N., Leat, P.T., Dickin, A.P., Morrison, M.A., Hendry, G.L. and Gibson, S.A., 1990. Strongly potassic mafic magmas from lithospheric mantle sources during continental extension and heating: evidence from Miocene minettes of northwest Colorado, U.S.A. Earth Planet. Sci. Lett., 98: 139–153.

Treuil, M. and Varet, J., 1973. Critères volcanologiques, pétrologiques et géochimiques de la genèse et de la différenciation des magmas basaltiques: exemple de l'Afar. Bull. Soc. Géol. Fr., 15: 401–644.

Treuil, M., Jaffrezic, H., Deschamps, N., Derre, C., Guichard, F., Joron, J.L., Pelletier, B., Novotny, S. and Courtois, C., 1973. Analyse des lanthanides, du hafnium, du scandium, du chrome, du manganèse, du cobalt, du cuivre et du zinc dans les minéraux et les roches par activation neutronique. J. Radioanal. Chem., 18: 55–68.

Treuil, M., Joron, J.L., Jaffrezic, H., Villemant, B. and Calas, G., 1979. Géochimie des éléments hygromagmatophiles, coefficients de partage minéraux/liquides et propriétés structurales de ces éléments dans les liquides magmatiques. Bull. Minéral., 102: 402–409.

Vai, G.B., 1989. Pre-Jurassic strike-slip rift pulses in circum-Mediterranean Western Tethyan realm. Proc. 28th Int. Geol. Congr., Washington, D.C., 3: 272–274.

Venturelli, G., Capedri, S., Di Battistini, G., Crawford, A., Kogarko, L.N. and Celestini, S., 1984a. The ultrapotassic rocks from Southeastern Spain. Lithos, 17: 37–54.

Venturelli, G., Thorpe, R.S., Dal Piaz, G.V., Del Moro, A. and Potts, P.J., 1984b. Petrogenesis of calc-alkaline, shoshonitic and associated ultrapotassic Oligocene volcanic rocks from the Northwestren Alps, Italy. Contrib. Mineral. Petrol., 86: 209–220.

Vidal, Ph., Cocherie, A. and Le Fort, P., 1982. Geochemical investigations of the origin of the Manaslu leucogranite (Himalaya, Nepal). Geochim. Cosmochim. Acta, 6: 2279–2292.

Vidal, Ph., Bernard-Griffiths, J., Cocherie, A., Le Fort, P., Peucat, J.J. and Sheppard, S.M.F., 1984. Geochemical comparison between Himalayan and Hercynian leucogranites. Phys. Earth Planet. Inter., 35: 179–190.

Wass, S.Y. and Rogers, N.W., 1980. Mantle metasomatism — precursor to continental alkaline volcanism. Geochim. Cosmochim. Acta, 44: 1811–1823.

Weiss, D., Demaiffe, D., Cauet, S. and Javoy, M., 1987. Sr, Nd, O and H isotopic ratios in Ascension Island lavas and plutonic inclusions; cogenetic origin. Earth Planet Sci. Lett., 82: 255–268.

Wildeman, T.R. and Condie, K.C., 1973. Rare earths in Archean graywackes from Wyoming and from the Fig Tree Group, South Africa. Geochim. Cosmochim. Acta, 37: 439–453.

Wildeman, T.R. and Haskin, L.A., 1973. Rare earth in Precambrian sediments. Geochim. Cosmochim. Acta, 37: 419–438.

Windom, K.E. and Boettcher, A.L., 1980. Mantle metasomatism and the kimberlite–lamprophyre association: evidence from an eclogite nodule from Roberts Victor Mine, South Africa. J. Geol., 88: 705–712.

Winkler, H.G.F., 1967. Petrogenesis of Metamorphosed Rocks. Springer, Berlin, rev. 2nd ed., 237 pp.

Wood, D.A., Joron, J.L., Treuil, M., Norry, M. and Tarney, J., 1979. Elemental and Sr isotope variations in basic lavas from Iceland and the surrounding ocean floor. Contrib. Mineral. Petrol., 70: 319–339.

Zorpi, M.J., Coulon, C. and Orsini, J.B., 1991. Hybridization between felsic and mafic magmas in calc-alkaline granitoids — a case study in northern Sardinia, Italy. In: A. Peccerillo (Guest-Editor), Geochemistry of Granitoid Rocks. Chem. Geol., 92: 45–86 (special issue).